

**Cell Biology:**

**After Embedding in Membranes  
Antiapoptotic Bcl-XL Protein Binds Both  
Bcl-2 Homology Region 3 and Helix 1 of  
Proapoptotic Bax Protein to Inhibit  
Apoptotic Mitochondrial Permeabilization**

Jingzhen Ding, Blaine H. M. Mooers, Zhi  
Zhang, Justin Kale, Domina Falcone, Jamie  
McNichol, Bo Huang, Xuejun C. Zhang,  
Chengguo Xing, David W. Andrews and  
Jialing Lin

*J. Biol. Chem.* published online March 10, 2014

CELL BIOLOGY

MEMBRANE  
BIOLOGY

Access the most updated version of this article at doi: [10.1074/jbc.M114.552562](https://doi.org/10.1074/jbc.M114.552562)

Find articles, minireviews, Reflections and Classics on similar topics on the [JBC Affinity Sites](#).

Alerts:

- [When this article is cited](#)
- [When a correction for this article is posted](#)

[Click here](#) to choose from all of JBC's e-mail alerts

This article cites 0 references, 0 of which can be accessed free at  
<http://www.jbc.org/content/early/2014/03/10/jbc.M114.552562.full.html#ref-list-1>

After Embedding in Membranes Antiapoptotic Bcl-XL Protein Binds Both Bcl-2 Homology Region 3 and Helix 1 of Proapoptotic Bax Protein to Inhibit Apoptotic Mitochondrial Permeabilization\*

Jingzhen Ding<sup>1</sup>, Blaine H. M. Mooers<sup>1,2</sup>, Zhi Zhang<sup>1</sup>, Justin Kale<sup>3</sup>, Domina Falcone<sup>3</sup>, Jamie McNichol<sup>3</sup>, Bo Huang<sup>4</sup>, Xuejun C. Zhang<sup>4</sup>, Chengguo Xing<sup>5</sup>, David W. Andrews<sup>3,6</sup>, and Jialing Lin<sup>1,2</sup>

From the <sup>1</sup>Department of Biochemistry and Molecular Biology, <sup>2</sup>Peggy and Charles Stephenson Cancer Center, University of Oklahoma Health Sciences Center, Oklahoma City, Oklahoma 73126, <sup>3</sup>Department of Biochemistry and Biomedical Sciences, McMaster University, Hamilton, Ontario L8N 3Z5, Canada, <sup>4</sup>Institute of Biophysics, Chinese Academy of Sciences, Beijing 100101, China, <sup>5</sup>Department of Medicinal Chemistry, University of Minnesota, Minneapolis, MN 55455 and <sup>6</sup>Biological Sciences, Sunnybrook Research Institute and Department of Biochemistry, University of Toronto, Toronto, Ontario, M4N 3M5, Canada.

Running title: *Architecture of antiapoptotic Bcl-XL:Bax dimer in membranes*

To whom correspondence should be addressed: Jialing Lin, 940 Stanton L. Young Blvd., Biomedical Sciences Bldg. 935, P.O. Box 26901, Oklahoma City, OK 73126-0901. Tel.: (405) 271-2227 (ext. 61216); Fax: (405) 271-3092; E-mail: [jialing-lin@ouhsc.edu](mailto:jialing-lin@ouhsc.edu)

**Keywords:** Bcl-2 proteins; Bcl-XL; Bax; mitochondrial apoptosis; membrane proteins; protein cross-linking

**Background:** Bcl-XL binds Bax at mitochondria inhibiting Bax oligomerization and apoptosis.

**Results:** Anchored in membranes, Bcl-XL:Bax heterodimer is formed from a rigid helix-in-groove interface plus a flexible helical dimer interface.

**Conclusion:** Two interfaces contribute equally to the heterodimer stability required to inhibit Bax.

**Significance:** This novel kind of protein-protein interaction stabilizes the membrane-bound heterodimer that is pivotal to apoptosis regulation.

## ABSTRACT

Bcl-XL binds to Bax inhibiting Bax oligomerization required for mitochondrial outer membrane permeabilization (MOMP) during apoptosis. How Bcl-XL binds to Bax in the membrane is not known. Here, we investigated the structural organization of Bcl-XL:Bax complexes formed in the MOM, including the binding interface and membrane topology, using site-specific crosslinking, compartment-specific labeling, and computational modeling. We found that one heterodimer interface is formed by a specific interaction between the Bcl-2 homology 1-3 (BH1-3) groove of Bcl-XL and the BH3 helix of Bax as previously defined by the crystal

structure of a truncated Bcl-XL protein and a Bax BH3 peptide (PDB ID: 3PL7). We also discovered a novel interface in the heterodimer formed by equivalent interactions between the helix 1 regions of Bcl-XL and Bax when their helical axes are oriented either in parallel or antiparallel. The two interfaces are located on the cytosolic side of the MOM, whereas helix 9 of Bcl-XL is embedded in the membrane together with helices 5, 6, and 9 of Bax. Formation of the helix 1:helix 1 interface partially depends on the formation of the groove: BH3 interface because point mutations in the latter interface and addition of ABT-737, a groove-binding BH3 mimetic, blocked the formation of both interfaces. The mutations and ABT-737 also prevented Bcl-XL from inhibiting Bax oligomerization and subsequent MOMP, suggesting that the structural organization in which interactions at both interfaces contribute to the overall stability and functionality of the complex represents antiapoptotic Bcl-XL:Bax complexes in the MOM.

Proteins of the B-cell lymphoma 2 (Bcl-2)<sup>S</sup> family can interact in the mitochondrial outer

membrane (MOM) to regulate its permeability. These proteins contain one or more Bcl-2 homology (BH) motifs and either promote or inhibit the MOM permeabilization (MOMP) that initiates apoptosis. Bcl-2 associated X (Bax) and Bcl-2 antagonist/killer 1 (Bak) contain three BH motifs (BH1-3) that are required for the MOMP and a six-residue structural motif similar to that found in the BH4 motif of antiapoptotic family members (1). Bcl-2, B-cell lymphoma-extra large (Bcl-XL), and other antiapoptotic family members contain four BH motifs (BH1-4), and function as both direct and indirect inhibitors of Bax and Bak. BH3-only proteins, such as BH3 interacting-domain death agonist (Bid), Bcl-2-like protein 11 (Bim), and Bcl-2-associated death promoter (Bad), contain only the BH3 motif, and promote the MOMP by activating Bax and Bak, inhibiting the antiapoptotic family members, or both (2-4).

Bax is inactive in the cytosol of normal cells but becomes active in apoptotic cells by changing conformation in a multi-step process. First, Bax is recruited to the mitochondria by truncated Bid (tBid) in the MOM (5,6). The membrane-bound Bax recruits more soluble Bax to the MOM by autoactivation (7). These Bax proteins bind to each other to form an oligomeric pore in the membrane. The oligomerization most likely takes place after Bax changes to a multispanning conformation with helices 5, 6, and 9 embedding in the membrane (8). The structure of the oligomeric Bax pore in the membrane is largely unknown. However, the data from several recent studies suggest a possible consensus structure. Our photocrosslinking study revealed two interdependent interfaces in the Bax oligomer that was formed in detergent micelles. The first one is formed by the BH1-3 regions, and the second one by helix 1 plus the following loop and helix 6 (9). An electron paramagnetic resonance study of Bax oligomers that were formed in detergent micelles and liposomal membranes together with homology modeling of the Bax dimer using a Bak dimer model suggested an antiparallel helical dimer interface formed by the helices 2-3 region of neighboring Bax molecules in the oligomer (10,11). A disulfide crosslinking study indicated that the helices 2-3 interface was extended to include helix 4, which binds to other side of helix 2, resulting in a BH3-in-groove dimer interface (12). This interface was also observed in

a crystallographic study using a Bax fragment containing helices 2 through 5 region (13). The BH3-in-groove dimer interface together with another parallel helical dimer interface formed by helix 6 of neighboring Bax molecules could generate a Bax oligomer in the MOM (12).

To inhibit Bax oligomerization, Bcl-XL could inhibit any one or more of these Bax homo-interactions, thereby interrupting the activation process. In addition, it could also sequester tBid, preventing tBid from binding to and activating Bax. Neither of these potential inhibitory functions of Bcl-XL is mutually exclusive. Thus, interaction with Bax could inhibit the conformational change in Bax, preventing it from adopting the multispanning state, the oligomerization of the multispanning monomers, or both. Early mutational studies indicate that the BH1-3 motifs of Bcl-XL and the BH3 motif of Bax mediate their interaction. For example, replacement of Asp<sup>68</sup> with arginine (D68R) in the BH3 region of Bax greatly impaired its interaction with antiapoptotic family members (14). In addition, replacement of Gly<sup>138</sup> with alanine (G138A) in the BH1 region of Bcl-XL abolished its binding to Bax and inhibition of apoptosis (15,16). The crystal structure of a truncated Bcl-XL protein in complex with a peptide containing the BH3 region of Bax shows that the peptide binds as an amphipathic alpha helix to a hydrophobic groove formed by the BH1-3 regions of Bcl-XL (17). While all of these studies provide clues, the complex structure formed by the full-length Bcl-XL and Bax proteins in membranes remains elusive.

Bcl-XL, like Bax, is a soluble cytosolic or peripheral membrane protein in normal cells. Upon activation by membrane-bound tBid or Bax, Bcl-XL integrates into the MOM (5). The membrane topology of the active Bcl-XL is not known. However, the homologous Bcl-2 changes conformation during apoptosis initiation and this conformational change is required for its antiapoptotic activity (18-20).

The following questions about Bcl-XL:Bax interaction are important and have not been answered. Does Bcl-XL binding to Bax prevent Bax from changing to the multispanning state or does it prevent Bax oligomerization? Is the BH1-3 groove:BH3 helix interface in the crystal structure relevant to the Bcl-XL:Bax complex formed in the MOM? Are there additional regions

of Bcl-XL and Bax involved in the complex formation, as we previously detected in the Bcl-2:Bax complex that was formed in detergent micelles (21)? If a second interface, in addition to the groove: BH3 interface, forms in the membrane-bound Bcl-XL:Bax complex, can ABT-737, a BH3 peptide mimetic that binds to the BH1-3 groove of Bcl-XL in solution (22), still disrupt the Bcl-XL:Bax complex in the membrane? To address these questions, we systematically mapped the interface and the topology of the Bcl-XL:Bax heterodimer that was formed in membranes. We built structural models for the heterodimer based on the experimental data, and we tested these models with additional experiments that used mutational and functional assays. We also monitored the effect of ABT-737 on the membrane-bound heterodimer, particularly its effect on the formation of a non groove: BH3 interface. Together, these studies revealed critical structural features of a functional Bcl-XL:Bax heterodimer that was formed in the biological membranes. Our results demonstrate that the membrane-bound heterodimer has two interfaces, the conventional groove: BH3 interface seen in crystal, and a novel helix1: helix 1 interface which surprisingly can form in either a parallel or antiparallel fashion.

## EXPERIMENTAL PROCEDURES

**Materials** – Phospholipids were purchased from Avanti Polar Lipids. The MOM liposomes consisting of MOM-characteristic lipids were made as described (7). The Bax<sup>-/-</sup>/Bak<sup>-/-</sup> mitochondria were isolated from the livers of Bak knockout mice that also lack Bax as described (5). The Bax BH3 peptide that contains Bax residues 53-86 including the BH3 region was synthesized by Abgent as described (7). The full-length human Bax protein with or without a N-terminal His<sub>6</sub> (6H)-tag was expressed and purified as described (9,23). The plasmid for expression of the N-terminal 6H-tagged human Bcl-XL in *Escherichia coli* was modified from the pCYB3-Bcl-XL plasmid by inserting six histidine codons in between the first two codons of Bcl-XL. The full-length human Bcl-XL protein with or without the N-terminal 6H-tag was expressed and purified as described (5,23), except that the 6H-Bcl-XL eluted from the chitin column was purified using a Ni<sup>2+</sup>-nitrilotriacetic acid agarose column, and the

resulting protein was dialyzed in 20% (v/v) glycerol and 20 mM Tris/HCl, pH 8.0.

**Single-cysteine and single-lysine Bax and Bcl-XL mutants** – To construct plasmids for *in vitro* transcription and translation of Bax and Bcl-XL, we inserted the coding region of full-length human Bax or Bcl-XL into the vector pSPUTK (Stratagene). We created lysine-null (K0) Bax and Bcl-XL mutant plasmids by changing all of the lysine codons to arginine codons, and cysteine-null (C0) Bax and Bcl-XL mutant plasmids by changing all of the cysteine codons to alanine codons. We then created Bax and Bcl-XL mutant plasmids with a single lysine or cysteine codon at particular positions by mutating the corresponding codons in the K0 or C0 mutant plasmid to lysine or cysteine codon, respectively. These single-lysine or single-cysteine mutants were designated as K or C following a letter and a number that indicate the wild type residue and its position, e.g., Bax A183K and Bcl-XL V126C.

**MOMP (cytochrome c release) assay** – The assay was modified from that described previously (24). Wild-type and mutant Bax and Bcl-XL proteins were synthesized using Transcription/Translation (TNT) coupled SP6 RNA polymerase/reticulocyte lysate system (Promega). The resulting reaction containing the Bcl-XL protein (3  $\mu$ l), the Bax protein (3  $\mu$ l), or both was incubated with the Bax<sup>-/-</sup>/Bak<sup>-/-</sup> mitochondria (0.5 mg/ml total protein). Purified tBid protein (17 nM) (23) or Bax BH3 peptide (40  $\mu$ M) was added to the reactions to activate the Bcl-XL and Bax proteins. An adequate volume of buffer A (110 mM KOAc, 1 mM Mg(OAc)<sub>2</sub>, 25 mM HEPES, pH 7.5, and 2 mM glutathione) was added to each reaction to bring the total volume to 15  $\mu$ l. After incubation for 1 h at 37°C, the samples were centrifuged at 10,000 g for 10 min. The resulting pellet fractions were resuspended with 0.5% (v/v) Triton X-100 in phosphate buffered saline (PBS, pH 7.4) to the same volume as the supernatant (S) fractions and centrifuged again at 16,100 x g for 10 min to obtain the second supernatant fractions as the detergent-solubilized mitochondrial pellet (P) fractions. The amounts of cytochrome c in both S and P fractions were measured using the enzyme-linked immunosorbent assay (ELISA) with the antibody against mouse cytochrome c from R&D Systems per its protocol. The fraction of cytochrome c release was

calculated using the following formula: [cytochrome c in S] / ([cytochrome c in S] + [cytochrome c in P]).

*Apoptotic activity of Bax mutants in bax<sup>-/-</sup>/bak<sup>-/-</sup> mouse embryonic fibroblasts (MEFs)* – Phoenix cells were seeded in 100 mm dishes and MEFs in 96-well plates. The pBabe-MN-Bax-IRES-GFP plasmids containing wild-type Bax, Lys-null, or single-lysine mutants were constructed as described previously (9). Each plasmid (10 µg) was transfected into the Phoenix cells with Exgene500 (Fermentas) to package the plasmid into a replication-incompetent murine virus. The media containing the virus were harvested 24 h after the transfection, filtered with 0.2 µm filter, and then added into the MEFs. After 48 h of infection, the MEFs were treated with 0.5 or 2 µM etoposide for 24 h, and 3-channel images (GFP, Annexin V R-PE, and DRAQ5) were collected from 5 fields of view in each well. In each field, cells were identified via the DRAQ5 imaging, and measurements of emission intensity of green fluorescent protein (GFP) and Annexin V were taken per cell from their respective images. The total number of cells measured in the 5 fields of any well was used to calculate the Annexin V-positive percentage score for that well. The fraction of Annexin V-positive cells was determined for green cells (infected) and non-green cells (uninfected) separately. Expression of GFP alone from the internal ribosome entry site (IRES) sequence was somewhat toxic. The toxicity was shown in the *bax<sup>-/-</sup>/bak<sup>-/-</sup>* MEFs and poorly inhibited by Bcl-2 (data not shown); hence, the toxicity was probably not due to apoptosis. Because co-expression of wild-type Bax significantly increased the apoptosis as detected by Annexin V staining, the assay could clearly reveal the apoptotic activity of the Bax mutants relative to the wild-type Bax that was assayed in parallel.

*Disulfide and bismaleimidohexane (BMH) crosslinking* – [<sup>35</sup>S]Met-labeled single-cysteine Bax and Bcl-XL mutant proteins were synthesized in the wheat germ-based *in vitro* translation system as described (25). The resulting reaction containing the Bax protein (10 µl), the Bcl-XL protein (10 µl), or both were incubated at 37°C for 1.5 h with the MOM liposomes (4 mM total lipids) or for 1 h with the Bax<sup>-/-</sup>/Bak<sup>-/-</sup> mitochondria (0.5-0.7 mg/ml total proteins), 36-40 µM BH3 peptide

or 1.2 nM tBid protein, and 1 mM dithiothreitol (DTT), and an adequate volume of buffer A to bring the total reaction volume to 40 µl. A subset of the reactions included 50 µM of ABT-737. The resulting proteoliposomes were isolated by a sucrose gradient centrifugation as 250-µl fractions from the top of the gradient (20,23). The mitochondria with Bax, Bcl-XL, or both bound were pelleted by centrifugation and resuspended in 100-µl buffer A as described (5). These membrane fractions were treated with 1 mM NaAsO<sub>4</sub> to decrease residual DTT and then with redox catalyst copper (II)(1,10-phenanthroline)<sub>3</sub> (CuPhe; consisting of 0.3 mM CuSO<sub>4</sub> and 1 mM 1,10-phenanthroline) to induce disulfide crosslinking. After incubation on ice for 30 min, the oxidation reactions were quenched by 20 mM N-ethylmaleimide (NEM) and 100 mM ethylenediaminetetraacetic acid (EDTA). For the “0 min” controls, NEM and EDTA were added to the samples to block the disulfide crosslinking before the addition of CuPhe. To produce crosslinking with BMH, the proteoliposomes were incubated with 100 mM BMH at room temperature for 30 min, and then the crosslinking reactions were stopped by the addition of 50 mM β-mercaptoethanol. Both disulfide and BMH crosslinked samples were solubilized with 1% (v/v) Triton X-100 before precipitation with trichloroacetic acid. The resulting proteins were analyzed by SDS-PAGE under non-reducing or reducing condition. The radioactive proteins and their adducts in the gels were detected by phosphor-imaging with Fuji FLA-9000 image scanner.

*Photocrosslinking* – [<sup>35</sup>S]Met-labeled Bax or Bcl-XL proteins with a single N<sup>ε</sup>-(5-azido-2-nitrobenzoyl)-lysine (ANB-lysine) incorporated at specific locations were synthesized from RNA of the corresponding single-lysine Bax or Bcl-XL mutants using the wheat germ-based *in vitro* translation system as described (25,26). 10 µl of the resulting Bax or Bcl-XL proteins was incubated at 37°C for 1.5 h with 2.2 µM purified 6H-Bcl-XL or 6H-Bax protein, the MOM liposomes of 4 mM total lipids, and 36-40 µM BH3 peptide in a 20-µl reaction adjusted by buffer A. The proteoliposomes were isolated as described above and photolyzed to induce crosslinking via the ANB probe. The resulting photoadducts of the

[<sup>35</sup>S]Met-labeled protein and the 6H-tagged protein were solubilized in 0.25% (v/v) Triton X-100, enriched on Ni<sup>2+</sup>-nitrilotriacetic acid agarose, eluted and analyzed with reducing SDS-PAGE and phosphor-imaging.

*IASD labeling* – [<sup>35</sup>S]Met-labeled single-cysteine Bax or Bcl-XL mutant proteins were synthesized by using either the wheat germ- or reticulocyte lysate-based *in vitro* translation system as described (25,26). The resulting reactions containing the Bax protein (10 μl), the Bcl-XL protein (10 μl), or both were incubated at 37 °C for 1.5 h with the MOM liposomes with 4 mM total lipids, 36–40 μM BH3 peptide, and an adequate volume of buffer A to bring the total reaction volume to 40 μl. A subset of the reactions also included 0.5 μM purified recombinant Bax or Bcl-XL protein. The resulting proteoliposomes were isolated as described above, and labeled with 0.2 mM (4-acetamido-4'[(iodoacetyl)amino]stilbene-2,2'-disulfonic acid (IASD) at room temperature in dark for 30 min in the absence or presence of 2% (w/v) 3-[(3-Cholamidopropyl)dimethylammonio]-1-propanesulfonate (CHAPS), 4 M urea, or both. The reactions were quenched by the addition of 10 mM β-mercaptoethanol. For the “0 min” controls, the β-mercaptoethanol was added before the addition of IASD to prevent the labeling. The radioactive IASD-labeled proteins were resolved from the unlabeled ones by isoelectric focusing (IEF) (8) and detected by phosphor-imaging. The intensities of the IASD-labeled and unlabeled bands for each protein under each condition were quantified using program ImageQuant from Fuji. The integrated intensities were used to calculate the fraction of IASD-labeling according to the following formula: intensity of labeled band(s) / (intensity of labeled band(s) + intensity of unlabeled band(s)).

*Modeling of Bcl-XL:Bax heterodimer interface and membrane topology* – The BH1-3 groove:BH3 helix interface for the Bcl-XL:Bax heterodimer was modeled based on the crystal structure of a Bcl-XL protein:Bax BH3 peptide complex (PDB ID: 3PL7) (17). The model was used to predict mutations that would disrupt the heterodimer interface, and the predictions were tested experimentally to verify the model.

The helix 1:helix 1 interface for the heterodimer was modeled based on the contact information of specific residues in these regions provided by the disulfide crosslinking experiments. The structure of Bax helix 1 was extracted from the NMR structure of a Bax monomer (PDB ID: 1F16) and then positioned in a parallel orientation with the Bcl-XL helix 1 in the Bcl-XL protein:Bax BH3 peptide complex structure (PDB ID: 3PL7) by interactive molecular modeling using program PyMOL (Schrodinger, LLC). Bad contacts between the two helices were relieved by changing the rotameric state of several side chains by using the Dunbrack backbone dependent rotamer library (27) via the mutagenesis wizard in PyMOL. The mutagenesis wizard was also used to change several residues to cysteines in order to fit the model to the disulfide crosslinking data. We used geometry regularization in program COOT (28) to remove any distortions in the backbone that were introduced while changing the amino acids. The stereochemical quality of the backbone was checked with a Ramachandran plot and the atom–atom clashes were scored using program MOLPROBITY in the presence of hydrogen atoms added using the electron-cloud X-H bond lengths (29). The modeling exercise was repeated with the Bax helix 1 rotated into an antiparallel orientation with the Bcl-XL helix 1 to fit with another set of disulfide crosslinking data. The parallel and antiparallel models were used as starting models in the Rosetta-based program FlexPepDock (30,31) to optimize the position of the peptide and the conformation of the side chains in and near the interface. Two hundred trial structures were generated and scored for each model. The ten trial structures with the most favorable scores were inspected with PyMOL. The parallel model and antiparallel model with the best agreement with the disulfide crosslinking data were selected for further analysis.

The overall structural organization model for the Bcl-XL:Bax heterodimer bound to the membrane was constructed from a composite of the BH1-3 groove:BH3 and parallel helix1:helix1 interface models described above. Helix 9 of Bcl-XL was built from the residues 206–230 using program PHYRE2 (32). Helices 4, 5, 6, 7, 8 and 9 of Bax were extracted from the Bax monomer structure (PDB ID: 1F16). Using PyMOL, these helices were added to the composite structure such

that the helix 9 of Bcl-XL and the helices 5, 6 and 9 of Bax were located under a virtual plane representing the cytosol-MOM boundary, while the helices 4, 7 and 8 of Bax were located above the plane with the composite structure. Further, the residues that were buried in the membrane as indicated by the IASD labeling results were placed under the plane, whereas the residues that were exposed to the aqueous milieu were placed above the plane. The positions of these helices relative to each other and to the composite structure were adjusted such that the distances between the indicated residues were in the range expected for the residues that could be crosslinked by BMH.

## RESULTS

*Experimental design* – The interface of Bcl-XL:Bax heterodimer that was formed in membranes was mapped using site-specific disulfide crosslinking and photocrosslinking. The former provided structural information about the interface at a higher resolution than the latter, because a disulfide bond can form only when the  $C_1^\beta$ - $C_2^\beta$  distance of the two cysteines are  $\sim 3$ - $5$  Å and the dihedral angle ( $C_1^\beta$ - $S_1^\gamma$ - $S_2^\gamma$ - $C_2^\beta$ ) about the disulfide bond is close to  $\pm 90^\circ$  (33). However, disulfide crosslinking occurs on a time scale of seconds to minutes (34,35) and may capture both the most abundant Bcl-XL:Bax complex that is in the most stable conformation and the rare complexes that are in less stable conformations and reached during the reaction time due to thermal fluctuations. In contrast, the photocrosslinking occurs within nanoseconds at a very low efficiency (36), thereby providing a “snapshot” of only the most stable and abundant complex while not sampling the less stable and rare complexes.

The topology of Bcl-XL:Bax heterodimer in membranes was determined by labeling the membrane-bound proteins with IASD, a sulfhydryl-reactive and membrane impermeant reagent with two negative charges. A cysteine in the protein that is exposed to the aqueous milieu will be labeled. On the other hand, a cysteine that is buried in a hydrophobic environment (e.g., a lipid bilayer, a protein core, or a protein complex interface) will not be labeled, unless a detergent such as CHAPS or a denaturant such as urea is

added to disrupt the bilayer or denature the protein or protein complex, respectively (8).

Two complementary *in vitro* membrane systems were used. First, the synthetic liposomal membrane consisting of the MOM-characteristic lipids but not proteins (7) simplified the data interpretation. Second, the isolated mitochondria provided a native environment for protein interactions for verification of the results from the liposome system.

To ensure that the structural information obtained from the above assays was from functional Bcl-XL:Bax complexes in membranes, only Bcl-XL and Bax mutants that were active in the MOMP assay were used in the crosslinking and labeling experiments. Moreover, mutations that could disrupt the heterodimer formation were generated, and their effects on inhibition of Bax-mediated MOMP by Bcl-XL were determined to define the structure-function relationship.

*The Bcl-XL and Bax mutants used in the interface- and topology-mapping experiments are functional* – In order to map the interface and topology of the Bcl-XL:Bax complex formed in membranes, we made Bcl-XL and Bax mutants with a single cysteine or lysine at specific locations (Fig. 1) (9). The mutant proteins were synthesized *in vitro* using a coupled transcription/translation system, and their MOMP activities were measured in an ELISA-based cytochrome c release assay (24). Each Bax mutant was activated by either purified tBid protein or a Bax peptide consisting of the BH3 region (BH3 peptide) and incubated with the mitochondria that lack both Bax and Bak (Bax<sup>-/-</sup>/Bak<sup>-/-</sup> mitochondria) either in the absence or presence of a Bcl-XL mutant. The resulting cytochrome c release was quantified. Like wild-type Bax, each single-cysteine Bax mutant released cytochrome c in a tBid- (Fig. 2A) or BH3 peptide- (data not shown) dependent manner. Like wild-type Bcl-XL, each single-cysteine Bcl-XL mutant inhibited the cytochrome c release by the single cysteine Bax mutant that was paired with the Bcl-XL mutant in the disulfide crosslinking experiments (Fig. 2A). The additional single-cysteine Bax and Bcl-XL mutants used in IASD labeling and BMH crosslinking experiments were also active (Fig. 2B). All of the single-lysine Bcl-XL mutants used in the photocrosslinking experiments had activities similar to that of the wild-type protein and the

lysine-null (K0) mutant (Fig. 2C). All of the single-lysine Bax mutants used in the photocrosslinking experiments were active in the MOMP assay (Fig. 2C), in Bax and Bak double knockout mouse embryonic fibroblast cells (*bax*<sup>-/-</sup>/*bak*<sup>-/-</sup> MEFs) (Fig. 2D), in HEK293 cells (9), or in both cells.

*In membranes, Bcl-XL and Bax dimerize via the canonical BH1-3 groove:BH3 helix interface after activation* – We performed disulfide crosslinking experiments to map the heterodimer interface using the active single-cysteine Bcl-XL and Bax proteins synthesized *in vitro*. We first did the experiments with the MOM liposomal membranes to avoid complications from the other mitochondrial proteins. We also used the Bax BH3 peptide instead of tBid to activate the soluble Bcl-XL and Bax proteins and generate the membrane-bound proteins, because tBid can bind to Bcl-XL and Bax in the membranes (5,6) and hence may interfere with the Bcl-XL:Bax interaction. Like tBid, the BH3 peptide could activate the Bcl-XL and Bax proteins (data not shown), but did not bind to the membranes as shown previously (7). As shown in Figure 3A, a disulfide-linked product with an apparent molecular mass ( $M_r$ ) close to that predicted for the Bcl-XL:Bax heterodimer was detected in the membranes when the indicated pairs of single-cysteine Bcl-XL and Bax mutants were targeted to the membranes. Particularly, the product (indicated by arrow in lane 2 or 10 on non-reducing gel) was formed when a Bcl-XL protein with the cysteine in the BH1-3 groove, V126C or L194C, was paired with a Bax protein with the cysteine in or near the BH3 region, L59C or M74C, respectively.

The following four results demonstrated that the arrow-indicated product was a disulfide-linked heterodimer of the single-cysteine Bcl-XL and Bax after they were activated by the BH3 peptide and targeted to the membranes. (i) The product appeared on the non-reducing gel and disappeared on the reducing gel (Fig. 3A, lanes 2 and 10), was not formed when the cysteine-null (C0) Bcl-XL and Bax mutants were used (Non-reducing, lane 4), and was greatly reduced when NEM was added to block the sulfhydryl moiety before oxidation by CuPhe (Non-reducing, lanes 1 vs. 2; 9 vs. 10). Therefore, it is a disulfide-linked product formed by the single-cysteine Bcl-XL and

Bax. (ii) The product was formed when both proteins were present in the membranes but not when one protein was omitted (Fig. 3A, Non-reducing, lanes 2 vs. 6 and 8; 10 vs. 12 and 14). Therefore, it is not a Bcl-XL or Bax homodimer. (iii) When one of the proteins was labeled by [<sup>35</sup>S]Met but the other was not, the product was still detectable but the radiation intensity was less than that when both proteins were labeled (Fig. 3B, the arrow-indicated bands in lanes 2 vs. 4 and 6; 8 vs. 10 and 12). These data suggest that the heterodimers detected in lanes 4 and 10 were formed by the radioactive Bcl-XL (visible in the phosphor-images, indicated by filled circles) and the nonradioactive Bax (invisible in the phosphor-images), and the heterodimers detected in lanes 6 and 12 were formed by the radioactive Bax (visible, indicated by open circles) and the nonradioactive Bcl-XL (invisible). In contrast, the heterodimers detected in lanes 2 and 8 were formed by the radioactive Bcl-XL and Bax that were both visible in the phosphor-images. (iv) When the BH3 peptide was omitted, although a substantial amount of Bcl-XL was bound to the membranes, the amount of Bax bound to the membranes was negligible, and the disulfide-linked heterodimer was undetectable in the membranes (Fig. 3C, lanes 6 and 14). In the absence of the membranes, virtually no Bcl-XL or Bax monomer was recovered from the membrane fraction in the sucrose gradient; neither was the disulfide-linked heterodimer (lanes 4 and 12). Therefore, the heterodimer detected in Figure 3A was formed by a disulfide-linkage of the indicated cysteines in the Bcl-XL and Bax proteins that were activated by the BH3 peptide and targeted to the membranes.

To verify whether the heterodimer interface detected in the liposomes after activation by the BH3 peptide is also formed in a more biological setting, we used tBid to activate the Bcl-XL and Bax proteins. Similar disulfide-linked heterodimers were formed in this system (Fig. 3D). Further, we targeted both proteins that were activated by the BH3 peptide to the *Bax*<sup>-/-</sup>/*Bak*<sup>-/-</sup> mitochondria, and detected similar disulfide-linked heterodimers (Fig. 3E and 3F). Therefore, the groove:BH3 interface is formed not only in the liposomal membranes, but also in the mitochondrial membranes after activation by either the BH3 peptide or the BH3 protein.

We also conducted photocrosslinking experiments using Bcl-XL and Bax mutants with a single photoreactive lysine analog located at specific positions. After activation by the BH3 peptide and targeting to the MOM liposomes, the *in vitro* synthesized [<sup>35</sup>S]Met-labeled Bcl-XL or Bax protein with the photoreactive probe, 5-azido-2-nitrobenzoyl (ANB), attached to the ε-amino group of the lysine located in or near the BH1-3 groove or the BH3 region crosslinked with the purified His<sub>6</sub>-tagged Bax or Bcl-XL protein, respectively (Fig. 4A and 4B). These data are consistent with those from disulfide crosslinking experiments and suggest the existence of the groove: BH3 interface in the Bcl-XL:Bax heterodimer that is formed in the membranes.

The above crosslinking data support a structural model in which the BH1-3 groove: BH3 helix interface, as seen previously by crystallography (17), exists in the Bcl-XL:Bax heterodimer formed in the MOM after both proteins are activated by the BH3 protein or peptide (Fig. 5). Clearly shown in the model, Val<sup>126</sup> and Leu<sup>194</sup> in the BH1-3 groove of Bcl-XL are in close proximity with Leu<sup>59</sup> and Met<sup>74</sup> in the BH3 helix of Bax, respectively (Fig. 5A). These hydrophobic residues interact to contribute a significant portion of the binding energy that holds the complex together. For example, Leu<sup>59</sup> and Met<sup>74</sup> in the BH3 helix of Bax bind to the first and the fifth hydrophobic pocket in the BH1-3 groove of Bcl-XL, respectively (17). Val<sup>126</sup> in the groove of Bcl-XL has van der Waals interaction with not only Leu<sup>59</sup> but also Leu<sup>63</sup>, which are the first and the second conserved hydrophobic residues in the BH3 region of Bax, respectively. The side chain of Leu<sup>194</sup> in the groove of Bcl-XL also has favorable van der Waals interactions with the aliphatic portion of the side chain of Arg<sup>78</sup> in the BH3 helix. When these Bcl-XL-Bax residue pairs are replaced by the cysteine pairs (V126C-L59C and L194C-M74C), the model predicts that the S<sub>1</sub><sup>γ</sup>-S<sub>2</sub><sup>γ</sup> distance between the paired cysteines and the C<sub>1</sub><sup>β</sup>-S<sub>1</sub><sup>γ</sup>-S<sub>2</sub><sup>γ</sup>-C<sub>2</sub><sup>β</sup> dihedral angle are close to the range for disulfide bond formation (Fig. 5B) (33). This prediction is supported by the disulfide crosslinking data (Fig. 3). The model also predicts that the C<sub>1</sub><sup>β</sup>-C<sub>2</sub><sup>β</sup> distance between Cys<sup>62</sup>, a native

cysteine located in the BH3 helix of Bax, and the Val<sup>126</sup> located in the groove of the Bcl-XL mutant is 9.8 Å (Fig. 5A), which is too great a distance to result in a disulfide bond when the Val<sup>126</sup> was changed to cysteine (V126C). Similar predictions were also made for the C<sub>1</sub><sup>β</sup>-C<sub>2</sub><sup>β</sup> distances between the other two mismatched cysteine pairs in the Bax-Bcl-XL complex: L59C-L194C and M74C-V126C (data not shown). These predictions were consistent with the observation that no disulfide-linked dimer was detected between the corresponding mismatched Bax-Bcl-XL mutant pairs (data not shown). It was also clear that the residues in the BH3 helix of Bax and the groove of Bcl-XL, which generated photocrosslinked heterodimers when replaced by ANB-lysine (Fig. 4), were located in or near the BH3:groove interface in the model (Fig. 5C).

*The helix 1 regions of Bcl-XL and Bax interact with each other in a parallel manner forming a novel interface in the heterodimer* – To determine if regions of Bcl-XL and Bax other than the BH1-3 regions are also involved in the heterodimerization, we used photocrosslinking to scan more Bcl-XL and Bax mutants with single ANB-lysine positioned in the other regions. The photoreactive probes located in helix 1 of both Bcl-XL and Bax generated the heterodimer-specific photoadducts in liposomes (Fig. 6), thereby indicating involvement of helix 1 in the heterodimerization. To determine if the helix 1 regions from both proteins interact with each other, we did disulfide crosslinking experiments with the following single-cysteine Bcl-XL-Bax mutant pairs: E7C-M20C, S18C-F30C, and S23C-R34C. After these mutants were activated by the BH3 peptide and targeted to the MOM liposomes (Fig. 7A) or the Bax<sup>-</sup>/Bak<sup>-</sup> mitochondria (Fig. 7B), multiple disulfide-linked products were detected, particularly in the mitochondria. Among these products, the ones marked with arrows are the Bcl-XL:Bax heterodimers because they were generated only when both proteins were targeted to the membranes and because their molecular masses were close to that of the heterodimer (Fig. 7A and 7B, lanes 6, 12 and 18). As expected, the heterodimer-specific bands were still detectable when one of the two proteins was not labeled with [<sup>35</sup>S]Met although the intensities of the bands were

weaker than those when both proteins were labeled in most cases (Fig. 7C, the arrow-indicated bands). When the BH3 peptide was omitted, although a substantial amount of Bcl-XL was bound to the liposomal membranes, the amount of Bax bound to the membranes was negligible, and the disulfide-linked heterodimers were undetectable in the membranes (Fig. 7D, lanes 6, 14 and 22). In the absence of the membranes, virtually no Bcl-XL or Bax monomer was recovered from the membrane fraction in the sucrose gradient; neither was the disulfide-linked heterodimer (Fig. 7D, lanes 4, 12 and 20). Therefore, the disulfide-linked heterodimers detected in Figure 7A and 7B were formed by the Bcl-XL and Bax mutants with the indicated cysteines in their helix 1 after they were activated by the BH3 peptide and targeted to the membranes.

When some single-cysteine Bcl-XL and Bax mutants were individually targeted to the membranes, disulfide-linked products were generated. Each of the products has a molecular mass close to that of the corresponding homodimer (Fig. 7A and 7B, indicated by filled or open triangles, respectively), suggesting that these products were disulfide-linked homodimers of Bcl-XL or Bax.

Additional disulfide-linked products were detected when certain single-cysteine Bcl-XL or Bax mutant was targeted to the mitochondria (Fig. 7B and 7C, indicated by stars and squares). These products were probably heterodimers of the respective single-cysteine mutant and mitochondrial proteins, because treatment of the mitochondria with NEM before targeting the single-cysteine mutant to the mitochondria and oxidation by CuPhe blocked the formation of these products (Fig. 7B, lanes 20 vs. 18; data not shown).

Using the disulfide crosslinking data from the single-cysteine Bcl-XL-Bax mutant pairs, E7C–M20C, S18C–F30C, and S23C–R34C, we built a molecular model for the helix 1:helix 1 interface in the Bcl-XL:Bax complex (Fig. 8A). We used the FlexPepDock program (30) to dock the helix 1 peptide from the NMR structure of Bax monomer (PDB ID: 1F16) against the helix 1 in Bcl-XL protein from the crystal structure of the Bcl-XL protein:Bax BH3 peptide complex (PDB ID: 3PL7). The two helix 1 regions, each with the

three cysteine substitutions, were aligned in parallel and positioned such that the  $C_1^\beta$ - $C_2^\beta$  distance and the  $C_1^\beta$ - $S_1^\gamma$ - $S_2^\gamma$ - $C_2^\beta$  dihedral angle in each cysteine pair were close to 4 Å and  $\pm 90^\circ$ , respectively, thus favoring the disulfide formation observed in the crosslinking experiments. We applied distance restraints in FlexPepDock program between the  $C^\beta$  atoms of the cysteine pairs, but the side chain conformations were not constrained to any target values. The FlexPepDock program generated 200 output models after ten cycles of optimizing the rigid body position and the backbone and side-chain conformations of the Bax helix 1 peptide and the side chain conformations of the Bcl-XL protein. The output models were ranked by their Rosetta energy scores (not shown). One of the top ten models is shown in the left panel of Figure 8A. The distribution of the scores was broad when plotted against the root-mean-square deviation with the starting model. In other words, the bottom of the docking funnel was flat. The top ten models differed in their scores by only 1-2 Rosetta energy units. In the selected model, the  $S_1^\gamma$ - $S_2^\gamma$  distances and the  $C_1^\beta$ - $S_1^\gamma$ - $S_2^\gamma$ - $C_2^\beta$  dihedral angles in the three cysteine pairs are near the ranges that allow disulfide formation (33).

We then replaced the three cysteine pairs in the structure shown in the left panel of Figure 8A with the corresponding wild-type residues and used the resulting structure as a starting model in FlexPepDock program to generate another 200 output models for the wild-type helix 1:helix 1 heterodimer interface. The right panel of Figure 8A depicts one of the top ten models, which predicts how Bcl-XL and Bax interact via their helix 1 when the two helices are parallel to each other. The model also indicates how the two helices form a previously unreported dimer interface that has the three wild-type Bcl-XL–Bax residue pairs, E7–M20, S18–F30, and S23–R34, in proximity to each other. The model predicted some stabilizing interactions including a hydrogen bond between the side chain  $N^\epsilon$  of Bax Arg<sup>34</sup> and the backbone carbonyl oxygen of Bcl-XL Gln<sup>19</sup>, and complete or partial burial of the hydrophobic side chains of Bax Leu<sup>26</sup>, Leu<sup>27</sup> and Phe<sup>30</sup> and

Ile<sup>31</sup>. These favorable interactions are countered by the burial of the negatively charged side chain of Bcl-XL Glu<sup>7</sup>. This model was also consistent with the photocrosslinking data because the residues that could form photoadducts, when replaced with ANB-lysine (Fig. 6), were also in or near the dimer interface (Fig. 8B).

*The helix 1 regions of Bcl-XL and Bax can also interact in an antiparallel fashion to form an alternative interface in the heterodimer* – To determine whether the helix 1:helix 1 heterodimer interface can form only in the parallel orientation, we did disulfide crosslinking experiments using mismatched single-cysteine mutant pairs that were activated by the BH3 peptide and targeted to the MOM liposomes. Surprisingly, Bcl-XL E7C or S23C mutant with the cysteine located near the N- or C-terminus of helix 1 formed a disulfide-linked dimer with Bax R34C or M20C with the cysteine located near the C- or N-terminus of helix 1, respectively (Fig. 9A). These disulfide crosslinking data support an "antiparallel dimer model" in which the two helix 1 regions from Bcl-XL and Bax are aligned antiparallel to each other (Fig. 9B). The model predicted stabilizing contributions from complete or partial burial of the hydrophobic side chains of Bcl-XL Val<sup>10</sup> and Trp<sup>24</sup> and Bax Ile<sup>19</sup>, Leu<sup>27</sup>, Phe<sup>30</sup> and Ile<sup>31</sup>. The Rosetta energy score (not shown) for the antiparallel model (Fig. 9B) was very close to that of the parallel model (Fig. 8A), suggesting that the helix 1:helix 1 dimer interface equally sampled the two arrangements of the Bax peptide. Further, the Rosetta energy scores calculated from the helix 1:helix 1 interface models were similar to that from the BH1-3 groove: BH3 helix interface model (Fig. 5A; data not shown), implying similar contributions from these interactions to the overall stability of the Bcl-XL:Bax complex. These Rosetta energy scores were also similar to those reported previously for the groove: BH3 interfaces formed by Bcl-XL and BH3 peptides from various BH3-only proteins (37), suggesting similar affinities for the binding of Bcl-XL to the Bax peptides and the BH3 peptides. On the other hand, the flexible binding interaction at the helix 1:helix 1 interface (Fig. 8A and 9B) contrasted with the rigid binding interaction at the groove: BH3 helix interface (Fig. 5A). We thus investigated their relationship and contribution to the function of the

Bcl-XL:Bax complex with the mutational analyses described below.

*The helix 1:helix 1 interaction is largely dependent on the BH1-3 groove: BH3 helix interaction, and both interactions are important for Bcl-XL to inhibit Bax-mediated MOMP* – To determine whether the novel helix 1:helix 1 interface can form independently of the canonical BH1-3 groove: BH3 helix interface, we tested several mutations that would disrupt the groove: BH3 interface and monitored their effect on both interfaces. According to the groove: BH3 interface model (Fig. 5A), Gly<sup>138</sup> in the groove of Bcl-XL has a favorable van der Waals interaction with Asp<sup>71</sup> in the BH3 helix of Bax. Replacement of the Gly<sup>138</sup> with alanine (G138A) would not only eliminate the van der Waals interaction but also generate a severe steric collision between the beta carbon of Ala<sup>138</sup> and the backbone carbonyl oxygen of Gly<sup>67</sup> in the BH3 helix of Bax (Fig. 10A, left panel). The next residue in the groove of Bcl-XL, Arg<sup>139</sup>, uses its side chain to form two hydrogen bonds as part of a strong salt bridge with the side chain of Asp<sup>68</sup> in the BH3 helix of Bax. Replacement of the Arg<sup>139</sup> with aspartate (R139D) would introduce a strong electrostatic repulsion with the Asp<sup>68</sup> of Bax and eliminate the strong salt bridge (Fig. 10A, left panel). On the Bax side, the side chain of Met<sup>74</sup> in the BH3 helix projects into the fifth hydrophobic pocket in the groove of Bcl-XL and forms favorable van der Waals interactions with the side chain of Tyr<sup>195</sup> in Bcl-XL. Replacement of the Met<sup>74</sup> with glutamate (M74E) would eliminate the hydrophobic interaction and generate a collision with the side chain of Tyr<sup>195</sup> (Fig. 10A, right panel). As predicted by the model, each mutation abolished the disulfide crosslinking of Bcl-XL with Bax in mitochondria via the V126C-L59C pair in the groove: BH3 interface (Fig. 10B, lanes 2 vs. 4, 5 and 6).

We then monitored the effects of the mutations in the groove: BH3 interface on the helix 1:helix 1 interface formation. Each of the mutations inhibited the disulfide crosslinking of Bcl-XL and Bax via the S23C-R34C pair in the parallel helix 1:helix 1 interface to a different extent (Fig. 10C). Thus, the M74E mutation in Bax BH3 helix completely abolished the crosslinking (lanes 6 vs. 8), whereas the R139D mutation in Bcl-XL groove inhibited the

crosslinking more than the G138A mutation (lanes 12 vs. 14 and 16). The three mutations also inhibited the hetero-disulfide crosslinking via the E7C-R34C and S23C-M20C pairs in the antiparallel helix 1:helix 1 interface to similar extents as those via the cysteine pair in the parallel interface (Fig. 10D, lanes 4 vs. 6, and 12 vs. 14 and 16). Therefore, the formation of the helix 1:helix 1 interface, no matter whether in the parallel or the antiparallel conformation, is at least partially dependent on the formation of the groove: BH3 interface.

We did the MOMP assay to test whether the physical disruption of the interfaces by the mutations impacted the inhibition of Bax-mediated MOMP by Bcl-XL. As shown in Figure 10E, Bcl-XL with V126C in the BH1-3 groove greatly inhibited the MOMP activity of Bax with L59C in the BH3 helix, whereas Bcl-XL with S23C or E7C in the helix 1 greatly inhibited the activity of Bax with R34C in the helix 1 (columns 1-3, and 9-12). However, the single-cysteine Bcl-XL mutants barely inhibited the MOMP activity of the corresponding single-cysteine Bax mutants that also have the M74E mutation (columns 4-6, and 13-16). Along with the great reduction in Bcl-XL's activity against the Bax-mediated MOMP, the M74E mutation in Bax also greatly impaired the formation of both the groove: BH3 helix interface and the helix 1:helix 1 interface, either parallel or antiparallel, as shown by the disulfide crosslinking data (Fig. 10B, lanes 2 vs. 4; 10C, lanes 6 vs. 8; and 10D, lanes 4 vs. 6). Similarly, when the R139D mutation was introduced into Bcl-XL V126C and S23C, the resulting Bcl-XL mutants partially lost the inhibitory activity on Bax L59C- and R34C- or M20C-mediated MOMP, respectively (Fig. 10E, columns 3 vs. 7 and 11 vs. 17 or 21 vs. 22). Consistent with the partial loss of Bcl-XL's activity against the Bax-mediated MOMP, the R139D mutation in Bcl-XL blocked the helix 1:helix 1 interaction to a lesser extent compared to the M74E mutation in Bax (Fig. 10C, lanes 6 vs. 8 and 12 vs. 16; 10D, lanes 4 vs. 6 and 12 vs. 16), although the two mutations blocked the groove: BH3 helix interaction equally (Fig. 10B, lanes 2 vs. 4 and 8). Interestingly, the effect of the G138A mutation in Bcl-XL on its inhibition of Bax-mediated MOMP depended on the cysteine location in the mutants. While the G138A mutation caused a partial loss in the Bcl-

XL V126C inhibition of Bax L59C (Fig. 10E, columns 3 vs. 8), it did not affect the Bcl-XL S23C inhibition of Bax R34C or M20C (Fig. 10E, columns 11 vs. 18 or 21 vs. 23). The differential effects of the G138A mutation on the anti-Bax activity of Bcl-XL in the MOMP could be explained by the differential effects of the mutation on the physical interaction of Bcl-XL with Bax. Thus, as indicated by the disulfide crosslinking data, the G138A mutation largely disrupted the groove: BH3 helix interaction between Bcl-XL V126C and Bax L59C (Fig. 10B, lanes 2 vs. 6), but only slightly inhibited the helix 1:helix 1 interaction between Bcl-XL S23C and Bax R34C or M20C (Fig. 10C, lanes 12 vs. 14; 10D, lanes 12 vs. 14). Therefore, the MOMP activity data from these Bcl-XL and Bax mutants are directly correlated with the physical interaction data, supporting a conclusion that the physical interactions in both interfaces are important for Bcl-XL to inhibit Bax-mediated MOMP.

*The BH1-3 groove of Bcl-XL directly competes with the BH1-3 groove of Bax for binding to the BH3 helix of Bax to inhibit Bax homo-oligomerization in the MOM* – The effects of the mutations in the BH1-3 groove of Bcl-XL on its interaction with Bax and inhibition of Bax-mediated MOMP suggest a critical role for the groove in the function of Bcl-XL. Conceivably, the BH1-3 groove in Bcl-XL would compete with a similar groove in Bax that has been suggested to bind the BH3 helix of Bax nucleating Bax oligomerization in the MOM (13). To test this scenario directly, we monitored the effect of Bcl-XL on Bax homo-disulfide crosslinking via T56C in the BH3 helix and R94C the BH1-3 groove that was previously used to capture a Bax homodimer formed via the BH3 helix: groove interface (12,13). The single-cysteine Bax mutants formed a disulfide-linked homodimer after they were activated by the BH3 peptide and targeted to the MOM liposomes (Fig. 11A, lane 2, indicated by open triangle), consistent with the previous finding from the mitochondria isolated from the apoptotic cells that expressed the same Bax mutants (12). Addition of purified recombinant Bcl-XL protein to the reaction inhibited the disulfide crosslinking of the Bax mutants (Fig. 11A, lanes 4 vs. 2). To demonstrate that the inhibition is directly caused by the competition between the BH1-3 grooves of Bcl-XL and Bax for the same BH3 helix of Bax,

we added Bcl-XL E129C mutant with a single cysteine in the BH1-3 groove to the Bax T56C with a single cysteine in the BH3 helix. As predicted by the groove: BH3 helix interface model for Bcl-XL:Bax heterodimer (Fig. 5), Bcl-XL E129C formed a disulfide-linked heterodimer with Bax T56C after they were activated by the BH3 peptide and targeted to the MOM liposomes (Fig. 11B, lane 2, indicated by arrow), suggesting that the similar BH1-3 grooves in Bcl-XL and Bax can interact with the same residue in the BH3 helix of Bax resulting in a direct competition. As expected, the R139D mutation in the groove of Bcl-XL E129C largely inhibited the hetero-disulfide linkage with Bax T56C (Fig. 11B, lanes 6 vs. 2). The R139D mutation also partially abolished the inhibition of Bax T56C-mediated MOMP by Bcl-XL E129C (Fig. 11D, columns 1-3 vs. 5). Altogether, these experiments demonstrated that the inhibition of Bax MOMP activity by Bcl-XL is directly mediated by the competition between the Bax homo-interaction and the hetero-interaction with Bcl-XL in the MOM via the similar BH3 helix: BH1-3 groove interfaces.

*ABT-737 dissociates the membrane-bound Bcl-XL:Bax heterodimer and restores Bax homo-oligomerization and MOMP activity* – ABT-737, a BH3 mimic compound, binds to the BH1-3 groove of Bcl-XL and inhibits its interaction with BH3-only proteins (22,38-40). Because Bcl-XL binds to Bax not only through the BH1-3 groove: BH3 interface but also the helix 1: helix 1 interface, we tried to determine if ABT-737 could fully inhibit the Bcl-XL interaction with Bax in membranes. We first tested the effect of ABT-737 on the formation of the two interfaces. When ABT-737 was included in the reaction with Bcl-XL E129C, Bax T56C, the BH3 peptide and the MOM liposomes, it dramatically blocked the disulfide crosslinking of the two proteins in the membranes (Fig. 11B, lanes 2 vs. 4), suggesting that ABT-737 outcompetes the BH3 helix of Bax for interaction with the groove of Bcl-XL. As predicted from the dependency of helix 1: helix 1 interface formation on groove: BH3 interface formation, the compound also partially inhibited the disulfide crosslinking of Bcl-XL S23C and Bax R34C with the cysteines located in the helix 1: helix 1 interface (Fig. 11C, lanes 2 vs. 4). Moreover, the compound almost fully reversed the inhibition of the homo-disulfide crosslinking between Bax T56C and Bax R94C by

recombinant Bcl-XL (Fig. 11A, lanes 4 vs. 6), indicating that ABT-737 has freed the BH3 helix of Bax from the groove of Bcl-XL, which in turn binds to the BH1-3 groove of other Bax. Consistent with the ABT-induced reformation of the Bax homo-complex in the presence of Bcl-XL, the addition of ABT-737 almost completely reversed the Bcl-XL inhibition on the MOMP by BH3 peptide-activated Bax (Fig. 11D, columns 3 vs. 4, and 8 vs. 9).

*Heterodimerization of Bcl-XL and Bax does not alter their membrane topology* – To determine the topology of the Bcl-XL:Bax heterodimer bound to the liposomal membrane after activation by the BH3 peptide, we used the compartment-specific IASD labeling. We first did the experiments using Bcl-XL and Bax mutants with a single cysteine located in the interfacial regions. As shown in Figure 12A, in the presence of excess purified recombinant Bax protein, the *in vitro* synthesized Bcl-XL S18C or S23C with the cysteine in helix 1, or V126C with the cysteine in the BH1-3 groove, was labeled by IASD without using the detergent CHAPS to solubilize the membrane or the denaturant urea to destabilize the proteins or their complexes. Addition of CHAPS, urea or both did not increase the labeling significantly. Likewise, in the presence of excess purified recombinant Bcl-XL protein, the CHAPS and urea-independent IASD labeling was observed for the *in vitro* synthesized Bax F30C or R34C with the cysteine in helix 1, or L59C with the cysteine in the BH3 helix (Fig. 11B). Because most of the *in vitro* synthesized Bcl-XL or Bax should be in complex with the purified Bax or Bcl-XL in the presence of excess purified Bax or Bcl-XL, respectively, the IASD labeling data suggest that these interfacial residues in the Bcl-XL:Bax heterodimer are located outside of the membrane and are accessible from the aqueous milieu. In contrast, the IASD labeling of Bcl-XL L194C with the cysteine in the groove near the C-terminus of helix 8 (Fig. 12A), or Bax M74C with the cysteine near the C-terminus of the BH3 helix (Fig. 12B), was increased by the addition of CHAPS, urea, or both, indicating these residues are buried at least partially in the membrane, in the protein, or in the protein complex.

We next determined the effect of Bcl-XL on the location of helices 5, 6 and 9 of Bax. We

previously found that these three helices are embedded in the MOM in the activated mitochondrial Bax (8). As shown in the top panel of Figure 12C, in the presence of excess purified Bcl-XL, most of the *in vitro* synthesized, BH3 peptide-activated, and MOM liposome-bound Bax V121C, T140C, and S184C with the cysteine located in the helices 5, 6, and 9, respectively, were not labeled by IASD unless CHAPS was added to the reaction either by itself or together with urea. These results suggest that these three residues, and these three helices by inference, were buried in the membrane at least partially. Similar IASD labeling profiles were observed for the three Bax mutants when the Bcl-XL was absent (Fig. 12C, top panel), suggesting that the activated Bax, which was not in complex with Bcl-XL, had a membrane topology similar to that of the inactivated Bax, which was in complex with Bcl-XL. The fractions of IASD-labeled Bax in the absence or presence of Bcl-XL with or without CHAPS from two to five independent experiments were quantified and shown in the bottom panel of Figure 12C. These quantitative data indicate that Bcl-XL binding to Bax did not significantly alter the multispanning topology of the activated Bax in the membrane.

We also determined the effect of Bax on the location of helices 5, 6, and 9 of Bcl-XL, the three putative membrane-spanning helices based on the structural homology with Bax and with the bacterial pore-forming toxins (41,42). In the presence and absence of excess purified Bax, most of Bcl-XL T216C and V224C with the cysteine in helix 9 were not labeled by IASD in the absence of CHAPS and urea, and addition of either CHAPS or urea increased the labeling significantly (Fig. 12D, top panel). These results suggest that these residues, and helix 9 by inference, were buried partially in the membrane and partially in the protein or the protein complex. In contrast, most of Bcl-XL E153C and S164C with the cysteine in helices 5 and 6, respectively, were labeled by IASD in the absence of CHAPS and urea, and addition of CHAPS, urea, or both did not alter the labeling significantly. These results suggest that these two residues, and helices 5 and 6 by inference, were mostly exposed to aqueous milieu. The average fractions of IASD labeled Bcl-XL in the absence or presence of Bax with or without CHAPS from three to four independent

experiments (Figure 12D, bottom panel) indicated that Bax binding to Bcl-XL did not change the tail-anchored topology of Bcl-XL in the membrane. Based on all of the IASD labeling data, we concluded that (i) the presence of the other protein did not significantly alter the topology of Bax and Bcl-XL in the MOM liposomal membrane, (ii) Bax in the heterodimer was likely in the multispanning conformation whereas Bcl-XL was likely in the tail-anchored conformation, and (iii) the two interfaces in the heterodimer were largely located outside of the membrane.

In contrast to Bcl-XL, two bands were detected in the IEF gel for the *in vitro* synthesized Bax proteins, even in the absence of IASD labeling (Fig. 12B and 12C, lane 1 in all panels). The two bands were also observed with the cysteine-null (C0) Bax mutant in the absence of IASD labeling (Fig. 12E). When a positively or negatively charged residue in Bax C0 was changed to uncharged cysteine, the bands shifted accordingly in the IEF gel relative to the bands of Bax C0 (Fig. 12E). We suspected that a post-translational modification specific to the wheat germ-based *in vitro* translation system altered the isoelectric point of the Bax proteins, causing the differential migrations in the IEF gel, because the Bax C0 protein synthesized in the reticulocyte lysate-based system migrated as a single band (Fig. 12E). Nevertheless, the modified and unmodified Bax proteins were equally accessible to IASD labeling under most conditions (Fig. 12B and 12C).

*The overall structural organization of Bcl-XL: Bax heterodimer in the membrane* – Because both Bcl-XL and Bax have one or more helices embedded in the membrane, it is conceivable these helices may interact to form an additional heterodimer interface inside the membrane. We used various crosslinking methods to test this possibility. The photocrosslinking data from photoreactive probes located in these membrane-embedded helices indicate the proximity of these helices to the other protein in the heterodimer (Fig. 13). However, the disulfide crosslinking experiments with cysteine placed throughout these helices did not capture any heterodimer (data not shown), suggesting that the distances between these helices were too long to be bridged by a disulfide bond. In support of this notion, chemical crosslinking with BMH, a membrane-permeant

and sulfhydryl-reactive bifunctional reagent, generated a heterodimer between Bcl-XL T219C with the cysteine in helix 9 and Bax K123C, R134C or L181C with the cysteine in helix 5, 6 or 9, respectively (Fig. 14). Because the two sulfhydryl-reactive maleimides in BMH were spaced  $\sim 13$  Å apart, and the reactive nitrene in the photoreactive probe was  $\sim 12$  Å away from the C $^{\alpha}$  of the lysine, both photo and chemical crosslinking data were consistent with a model in which helix 9 of Bcl-XL is embedded together with helices 5, 6, and 9 of Bax in the membrane, without being close enough to form an additional heterodimer interface.

We also used chemical crosslinking to assess the distance between the cytosolic part and the membrane-embedded part of the Bcl-XL:Bax heterodimer. As shown in Figure 14, Bcl-XL T216C or T219C with the cysteine in helix 9 was crosslinked to Bax C62, M74C, or M79C with the cysteine in the BH3 helix by BMH, whereas Bcl-XL L194C with the cysteine in helix 8 was crosslinked to Bax R94C with the cysteine in helix 4. Thus, the distances between these paired cysteines were  $\sim 13$  Å. These experimentally determined distances, together with the information about the interface and the membrane topology, were used to build a cartoon model for the overall structural organization of the Bcl-XL:Bax heterodimer that was partially embedded in the membrane (Fig. 15).

## DISCUSSION

*The BH1-3 groove:BH3 helix interaction in the membrane-bound Bcl-XL:Bax heterodimer and the functional consequence* – Accumulating mutagenesis and structure data indicates that a Bcl-XL BH1-3 groove:Bax BH3 helix interface is the exclusive site of interaction between the two proteins and therefore responsible for inhibition of Bax by Bcl-XL. However, it was still unclear whether this interaction existed in the membrane-bound complex and how this interaction integrated into the inhibitory function of Bcl-XL on Bax-mediated MOMP. We used site-specific crosslinking approaches to systematically map the interface of Bcl-XL:Bax heterodimer formed at the natural and artificial MOM. Collectively, our data support a direct physical interaction between the hydrophobic BH1-3 groove of Bcl-XL and the

amphipathic BH3 helix of Bax for the membrane-bound proteins, with an interface similar to that revealed by crystallography for the soluble Bcl-XL protein and Bax BH3 peptide (17). These data included: (i) formation of disulfide bonds between cysteines in the groove of Bcl-XL and those in the BH3 helix of Bax; (ii) formation of heterodimer-specific photoadducts via ANB-labeled lysines in the groove and the BH3 helix; (iii) disruption of the groove:BH3 interaction by the mutations in the groove and the BH3 helix, and by the groove-binding compound ABT-737. Interestingly, previous studies showed that two of the mutations, G138A in Bcl-XL and M74E in Bax which inhibited the heterodimerization in membranes in our study, abolished Bcl-XL inhibition of Bax in cells (17,43). In addition, ectopic expression of Bax in cells enhances sensitivity to ABT-737 when Bcl-XL is present (44). Consistent with these findings, these mutations and ABT-737 reversed the Bcl-XL repression of Bax-mediated MOMP in our cell-free system, suggesting that the BH1-3 groove:BH3 helix interaction in the membrane-bound Bcl-XL:Bax heterodimer inhibits Bax.

It was suggested that the BH3 motif of Bax is exposed upon activation, resulting in Bax autoactivation and homo-oligomerization (5,9,10,12,13,24,45). The results presented here show that the BH3 motif of Bax is sequestered in the BH1-3 groove of Bcl-XL, and that this hetero-interaction inhibits Bax homo-interaction in membranes via its BH3:BH1-3 groove interface. Therefore, the binding of Bcl-XL to Bax could potentially neutralize two activities mediated by the BH3 motif of active Bax in membranes: (i) the recruitment of cytosolic Bax to the membranes by preventing Bax autoactivation, facilitating retrotranslocation of Bax from mitochondria to cytosol (46), or both, and (ii) the homo-oligomerization of membrane-bound Bax. Both of these activities are essential for Bax-mediated MOMP.

*The helix 1:helix 1 interaction in the membrane-bound Bcl-XL:Bax heterodimer and the functional implication* – Although it was well documented that the BH3 motifs of proapoptotic members of Bcl-2 family and the BH1-3 groove of antiapoptotic members dictate their binding affinities and specificities in solution (47-49), it was speculated that regions other than BH1-3 in

Bax and Bcl-XL may contribute to their hetero- and homo-interactions and functions. First, Bax homo-oligomerization is mediated not only by the BH1-3 regions, but also by helices 1 and 6, and the loop connecting helices 1 and 2 (9,10,12). Second, Bax activation by BH3-only proteins and autoactivation by previously activated Bax are mediated by a BH3-binding triggering pocket comprised of helices 1 and 6, and the loop connecting helices 1 and 2 (7,45,50,51). Third, the helix 1 of Bcl-XL, which overlaps with the BH4 region, is essential for binding to soluble Bax thereby preventing Bax from inserting into membranes and perhaps retrotranslocating Bax from membranes to cytosol, and hence required for Bcl-XL to inhibit Bax-mediated apoptosis (5,52). Fourth, the 6A7 epitope of Bax, which overlaps with the helix 1, is not accessible to the 6A7 antibody in the Bax sequestered by Bcl-XL in cells (39,53).

Here, we demonstrated that the helix 1 regions in membrane-bound Bax and Bcl-XL directly interacted with each other and contributed to the functionality of the membrane-bound heterodimer. In contrast to the rigid groove: BH3 interface, the helix 1: helix 1 interface is flexible. The groove and the BH3 helix are formed by well-organized structural elements that are ideal for forming a rigid binding interface. In contrast, the helix 1 in both proteins is connected to the rest of the protein by a long and unstructured loop that provides the freedom for the helices to sample different binding interfaces to achieve a flexible interaction. It will be interesting to explore whether and how the multiple BH and non-BH regions of Bcl-XL and Bax are involved in the interactions with other family members at membranes, because these interactions are expected to alter the functional Bcl-XL: Bax interaction according to our Embedded Together model (3,54). The assays established here will be valuable tools for these explorations.

Beside disulfide-linking to each other, Bcl-XL and Bax with single cysteine in the BH4/helix 1 region could be disulfide-linked to a few unknown mitochondrial proteins (Fig. 7), suggesting that this region of Bcl-XL and Bax might exert activities other than regulation of MOMP. Bcl-XL was shown to regulate mitochondrial membrane potential by modulating the activity of voltage-dependent anion channel

via an interaction that requires the BH4/helix 1 region (55). The soluble form of Bax, which was unable to promote MOMP, positively regulated mitochondrial fusion through interaction with mitofusin-2 (56). On the other side, the MOM-bound Bax, even when sequestered by Bcl-XL and unable to induce MOMP, promoted mitochondrial fission (39,57). Interaction between Bcl-XL and Bax may regulate their interactions with these and other mitochondrial proteins and the corresponding activities, some of which are intimately connected with apoptosis (58,59).

*Does the structural difference between the Bax homo-complex and the Bax: Bcl-XL hetero-complex explain their functional difference?* – In spite of the striking similarity in their monomeric structure, it is puzzling how Bcl-XL interacts with Bax and thereby halts the homo-oligomerization of Bax. It is also unclear why Bcl-XL cannot form large oligomeric pores in membranes but Bax can. Now it becomes even more perplexing that Bcl-XL and Bax interact at membranes via two interfaces, the canonical groove: BH3 helix interface and the novel helix 1: helix 1 interface, which potentially can mediate the formation of a higher order hetero-oligomer. However, the disruptive mutations in the former interface also partially disrupt the latter one, suggesting that the formation of the latter interface partially depends on the formation of the former one. One explanation of this result is that both interfaces are used to form a more stable heterodimer as shown in our overall structural model (Fig. 15). Alternatively, the binding mediated by one interface is too weak to extend the heterodimer that is formed by the other interface to a higher order oligomer. In addition, Bax homo-oligomers are likely formed by the monomers that are deeply embedded into membranes (8). In contrast, our topology data for the Bcl-XL: Bax hetero-complex (Fig. 12) suggest that while the embedding of the Bax in the hetero-complex in the membrane is similar to that of the Bax in the homo-complex, the embedding of Bcl-XL seems to be shallower compared to that of Bax. Therefore, the different conformations of Bcl-XL and Bax in the membrane may be another factor that distinguishes the activities of the two proteins in the membrane.

*Are Bcl-XL and Bcl-2 different?* – Besides the subcellular localization, the differences between Bcl-2 and Bcl-XL, two antiapoptotic

proteins with similar soluble domain structures, were implied in many ways. First, Bcl-2 and Bcl-XL have different binding spectrums to BH3-only proteins as well as to Bax and Bak (39,48). Second, Bcl-XL is more effective than Bcl-2 in inhibition of apoptosis in some cell types (60). Third, our ISAD labeling data suggest that the Bcl-XL in complex with Bax may be in the same tail-anchored conformation that it adopts when targeted to membranes in the absence of Bax. In contrast, the full antiapoptotic function of Bcl-2, including inhibition of Bax, requires a changed membrane-bound conformation (18,20). Fourth, we found that Bcl-2 can be converted to a Bax-like molecule through interaction with Bim and tBid, whereas a similar conversion of Bcl-XL was not detected at least in liposomes (61).

*Conclusions* – Our study revealed two interfaces in the membrane-bound Bcl-XL:Bax complex. The first one is rigid with the BH3 helix of Bax sequestered in the BH1-3 groove of Bcl-XL, whereas the second one is flexible with the two helices 1 interacting either in parallel or antiparallel. Formation of the second interface largely depends on the first one yet both contribute to the overall stability of the heterodimer that inhibits homo-oligomerization of Bax and subsequent MOMP. Therefore, the rigid BH3:groove interface positions the two helices 1 such that they form a flexible interface which contributes significantly to energetic stabilization of the membrane-bound Bcl-XL:Bax heterodimer that is pivotal to apoptosis regulation.

## REFERENCES

1. Kvansakul, M., Yang, H., Fairlie, W. D., Czabotar, P. E., Fischer, S. F., Perugini, M. A., Huang, D. C., and Colman, P. M. (2008) Vaccinia virus anti-apoptotic F1L is a novel Bcl-2-like domain-swapped dimer that binds a highly selective subset of BH3-containing death ligands. *Cell Death Differ* **15**, 1564-1571
2. Youle, R. J., and Strasser, A. (2008) The BCL-2 protein family: opposing activities that mediate cell death. *Nat. Rev. Mol. Cell Biol.* **9**, 47-59
3. Leber, B., Lin, J., and Andrews, D. W. (2007) Embedded together: the life and death consequences of interaction of the Bcl-2 family with membranes. *Apoptosis* **12**, 897-911
4. Chipuk, J. E., Moldoveanu, T., Llambi, F., Parsons, M. J., and Green, D. R. (2010) The BCL-2 family reunion. *Mol Cell* **37**, 299-310
5. Billen, L. P., Kokoski, C. L., Lovell, J. F., Leber, B., and Andrews, D. W. (2008) Bcl-XL inhibits membrane permeabilization by competing with Bax. *PLoS Biol.* **6**, e147
6. Lovell, J. F., Billen, L. P., Bindner, S., Shamas-Din, A., Fradin, C., Leber, B., and Andrews, D. W. (2008) Membrane binding by tBid initiates an ordered series of events culminating in membrane permeabilization by Bax. *Cell* **135**, 1074-1084
7. Tan, C., Dlugosz, P. J., Peng, J., Zhang, Z., Lapolla, S. M., Plafker, S. M., Andrews, D. W., and Lin, J. (2006) Auto-activation of the apoptosis protein Bax increases mitochondrial membrane permeability and is inhibited by Bcl-2. *J. Biol. Chem.* **281**, 14764-14775
8. Annis, M. G., Soucie, E. L., Dlugosz, P. J., Cruz-Aguado, J. A., Penn, L. Z., Leber, B., and Andrews, D. W. (2005) Bax forms multispinning monomers that oligomerize to permeabilize membranes during apoptosis. *EMBO J.* **24**, 2096-2103
9. Zhang, Z., Zhu, W., Lapolla, S. M., Miao, Y., Shao, Y., Falcone, M., Boreham, D., McFarlane, N., Ding, J., Johnson, A. E., Zhang, X. C., Andrews, D. W., and Lin, J. (2010) Bax forms an oligomer via separate, yet interdependent, surfaces. *J Biol Chem* **285**, 17614-17627
10. Bleicken, S., Classen, M., Padmavathi, P. V., Ishikawa, T., Zeth, K., Steinhoff, H. J., and Bordignon, E. (2010) Molecular details of Bax activation, oligomerization, and membrane insertion. *J Biol Chem* **285**, 6636-6647
11. Dewson, G., Kratina, T., Sim, H. W., Puthalakath, H., Adams, J. M., Colman, P. M., and Kluck, R. M. (2008) To trigger apoptosis, Bak exposes its BH3 domain and homodimerizes via BH3:groove interactions. *Mol. Cell* **30**, 369-380
12. Dewson, G., Ma, S., Frederick, P., Hockings, C., Tan, I., Kratina, T., and Kluck, R. M. (2012) Bax dimerizes via a symmetric BH3:groove interface during apoptosis. *Cell Death Differ* **19**, 661-670
13. Czabotar, P. E., Westphal, D., Dewson, G., Ma, S., Hockings, C., Fairlie, W. D., Lee, E. F., Yao, S., Robin, A. Y., Smith, B. J., Huang, D. C., Kluck, R. M., Adams, J. M., and Colman, P. M. (2013) Bax Crystal Structures Reveal How BH3 Domains Activate Bax and Nucleate Its Oligomerization to Induce Apoptosis. *Cell* **152**, 519-531
14. Fletcher, J. I., Meusburger, S., Hawkins, C. J., Riglar, D. T., Lee, E. F., Fairlie, W. D., Huang, D. C., and Adams, J. M. (2008) Apoptosis is triggered when prosurvival Bcl-2 proteins cannot restrain Bax. *Proc Natl Acad Sci U S A* **105**, 18081-18087
15. Desagher, S., Osen-Sand, A., Nichols, A., Eskes, R., Montessuit, S., Lauper, S., Maundrell, K., Antonsson, B., and Martinou, J. C. (1999) Bid-induced conformational change of Bax is responsible for mitochondrial cytochrome c release during apoptosis. *J Cell Biol* **144**, 891-901
16. Sedlak, T. W., Oltvai, Z. N., Yang, E., Wang, K., Boise, L. H., Thompson, C. B., and Korsmeyer, S. J. (1995) Multiple Bcl-2 family members demonstrate selective dimerizations with Bax. *Proc Natl Acad Sci U S A* **92**, 7834-7838
17. Czabotar, P. E., Lee, E. F., Thompson, G. V., Wardak, A. Z., Fairlie, W. D., and Colman, P. M. (2011) Mutation to Bax beyond the BH3 domain disrupts interactions with pro-survival proteins and promotes apoptosis. *J Biol Chem* **286**, 7123-7131

18. Dlugosz, P. J., Billen, L. P., Annis, M. G., Zhu, W., Zhang, Z., Lin, J., Leber, B., and Andrews, D. W. (2006) Bcl-2 changes conformation to inhibit Bax oligomerization. *EMBO J.* **25**, 2287-2296
19. Kim, P. K., Annis, M. G., Dlugosz, P. J., Leber, B., and Andrews, D. W. (2004) During apoptosis Bcl-2 changes membrane topology at both the endoplasmic reticulum and mitochondria. *Mol. Cell* **14**, 523-529
20. Peng, J., Tan, C., Roberts, G. J., Nikolaeva, O., Zhang, Z., Lapolla, S. M., Primorac, S., Andrews, D. W., and Lin, J. (2006) tBid elicits a conformational alteration in membrane-bound Bcl-2 such that it inhibits Bax pore formation. *J. Biol. Chem.* **281**, 35802-35811
21. Ding, J., Zhang, Z., Roberts, G. J., Falcone, M., Miao, Y., Shao, Y., Zhang, X. C., Andrews, D. W., and Lin, J. (2010) Bcl-2 and Bax interact via the BH1-3 groove-BH3 motif interface and a novel interface involving the BH4 motif. *J Biol Chem* **285**, 28749-28763
22. Oltersdorf, T., Elmore, S. W., Shoemaker, A. R., Armstrong, R. C., Augeri, D. J., Belli, B. A., Bruncko, M., Deckwerth, T. L., Dinges, J., Hajduk, P. J., Joseph, M. K., Kitada, S., Korsmeyer, S. J., Kunzer, A. R., Letai, A., Li, C., Mitten, M. J., Nettesheim, D. G., Ng, S., Nimmer, P. M., O'Connor, J. M., Oleksijew, A., Petros, A. M., Reed, J. C., Shen, W., Tahir, S. K., Thompson, C. B., Tomaselli, K. J., Wang, B., Wendt, M. D., Zhang, H., Fesik, S. W., and Rosenberg, S. H. (2005) An inhibitor of Bcl-2 family proteins induces regression of solid tumours. *Nature* **435**, 677-681
23. Yethon, J. A., Epand, R. F., Leber, B., Epand, R. M., and Andrews, D. W. (2003) Interaction with a membrane surface triggers a reversible conformational change in Bax normally associated with induction of apoptosis. *J. Biol. Chem.* **278**, 48935-48941
24. Kim, H., Tu, H. C., Ren, D., Takeuchi, O., Jeffers, J. R., Zambetti, G. P., Hsieh, J. J., and Cheng, E. H. (2009) Stepwise activation of BAX and BAK by tBID, BIM, and PUMA initiates mitochondrial apoptosis. *Mol Cell* **36**, 487-499
25. Lin, J., Liang, Z., Zhang, Z., and Li, G. (2001) Membrane topography and topogenesis of prenylated Rab acceptor (PRA1). *J. Biol. Chem.* **276**, 41733-41741
26. Zhang, Z., Lapolla, S. M., Annis, M. G., Truscott, M., Roberts, G. J., Miao, Y., Shao, Y., Tan, C., Peng, J., Johnson, A. E., Zhang, X. C., Andrews, D. W., and Lin, J. (2004) Bcl-2 homodimerization involves two distinct binding surfaces, a topographic arrangement that provides an effective mechanism for Bcl-2 to capture activated Bax. *J. Biol. Chem.* **279**, 43920-43928
27. Dunbrack, R. L., Jr., and Karplus, M. (1993) Backbone-dependent rotamer library for proteins. Application to side-chain prediction. *J Mol Biol* **230**, 543-574
28. Emsley, P., Lohkamp, B., Scott, W. G., and Cowtan, K. (2010) Features and development of Coot. *Acta Crystallogr D Biol Crystallogr* **66**, 486-501
29. Chen, V. B., Arendall, W. B., 3rd, Headd, J. J., Keedy, D. A., Immormino, R. M., Kapral, G. J., Murray, L. W., Richardson, J. S., and Richardson, D. C. (2010) MolProbity: all-atom structure validation for macromolecular crystallography. *Acta Crystallogr D Biol Crystallogr* **66**, 12-21
30. Raveh, B., London, N., and Schueler-Furman, O. (2010) Sub-angstrom modeling of complexes between flexible peptides and globular proteins. *Proteins* **78**, 2029-2040
31. London, N., Raveh, B., Cohen, E., Fathi, G., and Schueler-Furman, O. (2011) Rosetta FlexPepDock web server--high resolution modeling of peptide-protein interactions. *Nucleic Acids Research* **39**, W249-253
32. Kelley, L. A., and Sternberg, M. J. (2009) Protein structure prediction on the Web: a case study using the Phyre server. *Nature Protocols* **4**, 363-371
33. Ozhogina, O. A., and Bominaar, E. L. (2009) Characterization of the kringle fold and identification of a ubiquitous new class of disulfide rotamers. *Journal of Structural bBiology* **168**, 223-233

34. Braun, T. F., and Blair, D. F. (2001) Targeted disulfide cross-linking of the MotB protein of *Escherichia coli*: evidence for two H(+) channels in the stator Complex. *Biochemistry* **40**, 13051-13059
35. Trakselis, M. A., Alley, S. C., and Ishmael, F. T. (2005) Identification and mapping of protein-protein interactions by a combination of cross-linking, cleavage, and proteomics. *Bioconjug Chem* **16**, 741-750
36. Brunner, J. (1993) New photolabeling and crosslinking methods. *Annu. Rev. Biochem.* **62**, 483-514
37. London, N., Gulla, S., Keating, A. E., and Schueler-Furman, O. (2012) In silico and in vitro elucidation of BH3 binding specificity toward Bcl-2. *Biochemistry* **51**, 5841-5850
38. Aranovich, A., Liu, Q., Collins, T., Geng, F., Dixit, S., Leber, B., and Andrews, D. W. (2012) Differences in the mechanisms of proapoptotic BH3 proteins binding to Bcl-XL and Bcl-2 quantified in live MCF-7 cells. *Mol Cell* **45**, 754-763
39. Llambi, F., Moldoveanu, T., Tait, S. W., Bouchier-Hayes, L., Temirov, J., McCormick, L. L., Dillon, C. P., and Green, D. R. (2011) A unified model of mammalian BCL-2 protein family interactions at the mitochondria. *Mol Cell* **44**, 517-531
40. Lee, E. F., Czabotar, P. E., Smith, B. J., Deshayes, K., Zobel, K., Colman, P. M., and Fairlie, W. D. (2007) Crystal structure of ABT-737 complexed with Bcl-xL: implications for selectivity of antagonists of the Bcl-2 family. *Cell Death Differ* **14**, 1711-1713
41. Muchmore, S. W., Sattler, M., Liang, H., Meadows, R. P., Harlan, J. E., Yoon, H. S., Nettesheim, D., Chang, B. S., Thompson, C. B., Wong, S. L., Ng, S. L., and Fesik, S. W. (1996) X-ray and NMR structure of human Bcl-xL, an inhibitor of programmed cell death. *Nature* **381**, 335-341
42. Suzuki, M., Youle, R. J., and Tjandra, N. (2000) Structure of Bax: coregulation of dimer formation and intracellular localization. *Cell* **103**, 645-654
43. Otilie, S., Diaz, J. L., Chang, J., Wilson, G., Tuffo, K. M., Weeks, S., McConnell, M., Wang, Y., Oltersdorf, T., and Fritz, L. C. (1997) Structural and functional complementation of an inactive Bcl-2 mutant by Bax truncation. *J Biol Chem* **272**, 16955-16961
44. Gautier, F., Guillemain, Y., Cartron, P. F., Gallenne, T., Cauquil, N., Le Diguarher, T., Casara, P., Vallette, F. M., Manon, S., Hickman, J. A., Geneste, O., and Juin, P. (2011) Bax activation by engagement with, then release from, the BH3 binding site of Bcl-xL. *Mol Cell Biol* **31**, 832-844
45. Gavathiotis, E., Reyna, D. E., Davis, M. L., Bird, G. H., and Walensky, L. D. (2010) BH3-triggered structural reorganization drives the activation of proapoptotic BAX. *Mol Cell* **40**, 481-492
46. Edlich, F., Banerjee, S., Suzuki, M., Cleland, M. M., Arnoult, D., Wang, C., Neutzner, A., Tjandra, N., and Youle, R. J. (2011) Bcl-x(L) retrotranslocates Bax from the mitochondria into the cytosol. *Cell* **145**, 104-116
47. Certo, M., Del Gaizo Moore, V., Nishino, M., Wei, G., Korsmeyer, S., Armstrong, S. A., and Letai, A. (2006) Mitochondria primed by death signals determine cellular addiction to antiapoptotic BCL-2 family members. *Cancer Cell* **9**, 351-365
48. Chen, L., Willis, S. N., Wei, A., Smith, B. J., Fletcher, J. I., Hinds, M. G., Colman, P. M., Day, C. L., Adams, J. M., and Huang, D. C. S. (2005) Differential targeting of prosurvival Bcl-2 proteins by their BH3-only ligands allows complementary apoptotic function. *Mol. Cell* **17**, 393-403
49. Kuwana, T., Bouchier-Hayes, L., Chipuk, J. E., Bonzon, C., Sullivan, B. A., Green, D. R., and Newmeyer, D. D. (2005) BH3 domains of BH3-only proteins differentially regulate Bax-mediated mitochondrial membrane permeabilization both directly and indirectly. *Mol Cell* **17**, 525-535
50. Cartron, P.-F., Gallenne, T., Bougras, G., Gautier, F., Manero, F., Vusio, P., Meflah, K., Vallette, F. M., and Juin, P. (2004) The first alpha helix of Bax plays a necessary role in its ligand-induced activation by the BH3-only proteins Bid and PUMA. *Mol. Cell* **16**, 807-818

51. Gavathiotis, E., Suzuki, M., Davis, M. L., Pitter, K., Bird, G. H., Katz, S. G., Tu, H. C., Kim, H., Cheng, E. H., Tjandra, N., and Walensky, L. D. (2008) BAX activation is initiated at a novel interaction site. *Nature* **455**, 1076-1081
52. Zhou, H., Hou, Q., Chai, Y., and Hsu, Y. T. (2005) Distinct domains of Bcl-XL are involved in Bax and Bad antagonism and in apoptosis inhibition. *Exp Cell Res* **309**, 316-328
53. Hsu, Y. T., Wolter, K. G., and Youle, R. J. (1997) Cytosol-to-membrane redistribution of Bax and Bcl-X(L) during apoptosis. *Proc. Natl. Acad. Sci. U. S. A.* **94**, 3668-3672
54. Leber, B., Lin, J., and Andrews, D. W. (2010) Still embedded together binding to membranes regulates Bcl-2 protein interactions. *Oncogene* **29**, 5221-5230
55. Shimizu, S., Konishi, A., Kodama, T., and Tsujimoto, Y. (2000) BH4 domain of antiapoptotic Bcl-2 family members closes voltage-dependent anion channel and inhibits apoptotic mitochondrial changes and cell death. *Proc. Natl. Acad. Sci. USA* **97**, 3100-3105
56. Hoppins, S., Edlich, F., Cleland, M. M., Banerjee, S., McCaffery, J. M., Youle, R. J., and Nunnari, J. (2011) The soluble form of Bax regulates mitochondrial fusion via MFN2 homotypic complexes. *Mol Cell* **41**, 150-160
57. Sheridan, C., Delivani, P., Cullen, S. P., and Martin, S. J. (2008) Bax- or Bak-induced mitochondrial fission can be uncoupled from cytochrome C release. *Mol Cell* **31**, 570-585
58. Suen, D. F., Norris, K. L., and Youle, R. J. (2008) Mitochondrial dynamics and apoptosis. *Genes Dev* **22**, 1577-1590
59. Tsujimoto, Y., and Shimizu, S. (2007) Role of the mitochondrial membrane permeability transition in cell death. *Apoptosis* **12**, 835-840
60. Fiebig, A. A., Zhu, W., Hollerbach, C., Leber, B., and Andrews, D. W. (2006) Bcl-XL is qualitatively different from and ten times more effective than Bcl-2 when expressed in a breast cancer cell line. *BMC Cancer* **6**, 213
61. Zhao, L., He, F., Liu, H., Zhu, Y., Tian, W., Gao, P., He, H., Yue, W., Lei, X., Ni, B., Wang, X., Jin, H., Hao, X., Lin, J., and Chen, Q. (2012) Natural diterpenoid compound elevates expression of Bim protein, which interacts with antiapoptotic protein Bcl-2, converting it to proapoptotic Bax-like molecule. *J Biol Chem* **287**, 1054-1065

*Acknowledgment* – We thank Jarkko Ylanko for helping with some of the data analysis, and Kathy Kyler for editing the manuscript.

## FOOTNOTES

\*This work was supported by NIH grant R01GM062964 and OCAST grant HR10-121 (to J. L.), NIH grants R01AI088011 and P20GM103640 (to B. H. M. M.) and CIHR grant FRN 12517 (to D. W. A. and Brian Leber). D. W. A. holds the Tier 1 Canada Research Chair in Membrane Biogenesis.

<sup>§</sup>The abbreviations used are: ANB, 5-azido-2-nitrobenzoyl; Bad, Bcl-2-associated death promoter; Bak, Bcl-2 antagonist/killer 1; Bax, Bcl-2 associated X; Bcl-2, B-cell lymphoma 2; Bcl-XL, B-cell lymphoma-extra large; BH, Bcl-2 homology; Bid, BH3 interacting-domain death agonist; Bim, Bcl-2-like protein 11; BMH, *bismaleimidohexane*; CHAPS, 3-[(3-cholamidopropyl)dimethylammonio]-1-propanesulfonate; CuPhe, copper (II)(1,10-phenanthroline)<sub>3</sub>; EDTA, ethylenediaminetetraacetic acid; ELISA, enzyme-linked immunosorbent assay; GFP, green fluorescent protein; IASD, (4-acetamido-4'[(iodoacetyl)amino]stilbene-2,2'-disulfonic acid; IEF, isoelectric focusing; IRES, internal ribosome entry site; MOM, mitochondrial outer membrane; MOMP, mitochondrial outer membrane permeabilization; NEM, N-ethylmaleimide; tBid, truncated Bid.

## FIGURE LEGENDS

Figure 1. **Sequences of Bax and Bcl-XL mutants.** *A-B*, single-cysteine Bax and Bcl-XL mutants. Bax (*A*) and Bcl-XL (*B*) sequences are shown with BH motifs highlighted by dashed lines above and helices identified by arrows below. The native cysteines (underlined Cs) were changed to alanine to create the cysteine-null (C0) mutants. Single-cysteine Bax and Bcl-XL mutants were created from the respective cysteine-null mutants by individually replacing the residues in bold with cysteine. Arrowheads indicate Met<sup>74</sup> of Bax, and Gly<sup>138</sup> and Arg<sup>139</sup> of Bcl-XL that were changed to glutamate, alanine and aspartate in Bax M74E, and Bcl-XL G138A and R139D mutants, respectively. *C*, single-lysine Bcl-XL mutants. Bcl-XL sequence is shown with BH motifs and helices indicated as in panel *B*. The native lysines (underlined Ks) were changed to arginine to create the lysine-null (K0) mutant. Single-lysine Bcl-XL mutants were created from the lysine-null mutant by individually replacing the residues in bold with lysine.

Figure 2. **Activities of Bax and Bcl-XL mutants in Bax<sup>-/-</sup>/Bak<sup>-/-</sup> mitochondria and mouse embryonic fibroblasts.** *A-C*, the MOMP activity in the Bax<sup>-/-</sup>/Bak<sup>-/-</sup> mitochondria. Wild-type (WT) or the indicated mutant Bax proteins were synthesized *in vitro*, activated by tBid protein and targeted to the Bax<sup>-/-</sup>/Bak<sup>-/-</sup> mitochondria in the absence or presence of WT or the indicated mutant Bcl-XL proteins that were synthesized *in vitro*. Cytochrome c release from the mitochondria was measured using ELISA. Data shown are average fractions of cytochrome c release from two to three independent experiments with the ranges indicated by error bars. *D*, the apoptotic activity of WT, lysine-null and single-lysine mutant Bax in the *bax<sup>-/-</sup>/bak<sup>-/-</sup>* MEFs. The MEF cells were infected with retrovirus that co-expressed Bax and GFP from the same message using the IRES sequence between the two coding regions, and treated with etoposide of the indicated concentrations. The cells were examined for apoptosis by Annexin V staining. Both panels show the fraction of adherent Annexin V-positive cells in the GFP-positive (infected and expressing Bax; black bar) and GFP-negative (uninfected and not expressing Bax; white bar) populations. The type of Bax protein expressed by the virus that was used to infect the cells is indicated below the plot. GFP indicates the control virus that expressed only GFP, and WT, K0, or K21, etc. indicate the virus that expressed GFP and wild-type, lysine-null, or single-lysine Bax, respectively. Data shown are the averages from eight independent replicates for each experiment with a minimum of 356 cells/well (average = 1084, max = 2613) and 309 cells/well (average = 849, max = 1442) analyzed for the upper and lower panel data, respectively. The error bars indicate one standard deviation.

Figure 3. **Disulfide crosslinking of Bax and Bcl-XL proteins with a single cysteine in BH3 helix and BH1-3 groove, respectively.** *A*, the *in vitro* synthesized [<sup>35</sup>S]Met-labeled cysteine-null and single-cysteine Bax and Bcl-XL proteins were activated by the BH3 peptide and targeted to the MOM liposomes. The resulting proteoliposomes were isolated and oxidized by CuPhe for 30 min. NEM and EDTA were then added to stop the oxidation. For the “0 min” controls, NEM and EDTA were added prior to the addition of CuPhe. The resulting samples were analyzed by non-reducing and reducing SDS-PAGE and phosphor-imaging. *B*, the *in vitro* synthesized radioactive (R) and/or non-radioactive (N) Bax and Bcl-XL mutants were activated by the BH3 peptide and targeted to the MOM liposomes. The resulting proteoliposomes were processed and analyzed as described in panel *A*. *C*, the *in vitro* synthesized radioactive Bax and Bcl-XL mutant proteins were incubated in the absence or presence of the MOM liposomes and/or the BH3 peptide. The resulting proteoliposomes were processed and analyzed as described in panel *A*. *D-E*, the *in vitro* synthesized radioactive Bax and Bcl-XL mutants were activated by tBid and targeted to the MOM liposomes (*D*) or activated by the BH3 peptide and targeted to the Bax<sup>-/-</sup>/Bak<sup>-/-</sup> mitochondria (*E*). The resulting membranes were isolated, oxidized and analyzed as described in panel *A*. *F*, the *in vitro* synthesized radioactive (R) and/or non-radioactive (N) Bax and Bcl-XL mutant proteins were activated by the BH3 peptide and targeted to the Bax<sup>-/-</sup>/Bak<sup>-/-</sup> mitochondria. The resulting mitochondria were isolated, oxidized and analyzed as described in panel *A*. In all panels, protein standards are indicated on the side of phosphor-images with their molecular masses (M<sub>r</sub>). Arrows indicate the disulfide-linked Bax:Bcl-XL heterodimers, and open or filled circles indicate the Bax or Bcl-XL monomers, respectively.

Figure 4. **Photocrosslinking of Bcl-XL or Bax mutant proteins with a single photoreactive ANB-lysine incorporated in BH1-3 groove or BH3 helix, respectively.** The *in vitro* synthesized [<sup>35</sup>S]Met-labeled Bcl-XL (*A*) or Bax (*B*) mutant proteins without lysine (K0) and with single photoreactive ANB probe incorporated at the indicated lysine positions (F97K, M79K, etc.) were mixed with the purified 6H-Bax (*A*) or 6H-Bcl-XL (*B*) protein. The proteins were activated by the BH3 peptide and targeted to the MOM liposomes. The resulting proteoliposomes were isolated and photolyzed. The resulting photoadducts of the 6H-tagged and the [<sup>35</sup>S]-labeled proteins were enriched and analyzed by reducing SDS-PAGE and phosphor-imaging. Protein standards are indicated on the side of phosphor-images with M<sub>r</sub>. The filled or open circle indicates the [<sup>35</sup>S]-Bcl-XL or [<sup>35</sup>S]-Bax monomer, respectively. The arrow indicates the photoadduct of [<sup>35</sup>S]-Bcl-XL and 6H-Bax (*A*) or [<sup>35</sup>S]-Bax and 6H-Bcl-XL (*B*).

Figure 5. **A model for the BH1-3 groove: BH3 helix interface in the membrane-bound Bcl-XL:Bax heterodimer.** *A*, the crystal structure of Bcl-XL protein:Bax BH3 peptide complex (PDB ID: 3PL7) is shown with V126–L59 and L194–M74, the residue pairs which formed disulfide bonds when they were replaced with cysteine pairs (Fig. 3), presented in stick form, and their beta carbon atoms (C<sub>1</sub><sup>β</sup> and C<sub>2</sub><sup>β</sup>) linked by dashed lines with the distances in Å indicated. Cys<sup>62</sup>, a native cysteine in the BH3 region of Bax, is also presented in stick form with its C<sup>β</sup> linked to the C<sup>β</sup> of Bcl-XL V126 and the distance in Å indicated. *B*, the two Bcl-XL–Bax residue pairs, V126–L59 and L194–M74, shown in panel *A* are replaced by two cysteine pairs, which are presented in stick form with their gamma sulfur atoms (S<sub>1</sub><sup>γ</sup> and S<sub>2</sub><sup>γ</sup>) linked by virtual bonds and the distances in Å indicated. The C<sub>1</sub><sup>β</sup>–S<sub>1</sub><sup>γ</sup>–S<sub>2</sub><sup>γ</sup>–C<sub>2</sub><sup>β</sup> dihedral angles about the V126C–L59C and L194C–M74C disulfide bonds are -52.2° and +22.0°, respectively. *C*, the crystal structure of Bcl-XL protein:Bax BH3 peptide complex is shown with the residues that generated the heterodimer-specific photoadducts when replaced by ANB-lysine (Fig. 4) presented in stick form. In all panels, the BH1, BH2, BH3, and BH4 regions of Bcl-XL protein are colored blue, cyan, red and orange, respectively, and the BH3 region of Bax peptide is colored green.

Figure 6. **Photocrosslinking of Bax and Bcl-XL mutant proteins with single photoreactive ANB-lysine incorporated in their helix 1.** The [<sup>35</sup>S]Met-labeled Bcl-XL (*A*) or Bax (*B*) mutant proteins with

single photo-reactive ANB probe incorporated at the indicated lysine positions were synthesized *in vitro*, and activated together with the purified 6H-Bax (A) or 6H-Bcl-XL (B) protein, respectively, by the BH3 peptide. The proteins were targeted to the MOM liposomes, processed and analyzed as described in Figure 4.

**Figure 7. Disulfide crosslinking of Bax and Bcl-XL proteins with a single cysteine in their helix 1.** A-B, the *in vitro* synthesized [<sup>35</sup>S]Met-labeled single-cysteine Bcl-XL and Bax proteins were activated by the BH3 peptide and targeted to the MOM liposomes (A) or the Bax<sup>-/-</sup>/Bak<sup>-/-</sup> mitochondria (B). The resulting membrane-bound proteins were processed and analyzed as described in Figure 3. C, the *in vitro* synthesized radioactive (R) and/or non-radioactive (N) single-cysteine Bcl-XL and Bax proteins were activated by the BH3 peptide and targeted to the Bax<sup>-/-</sup>/Bak<sup>-/-</sup> mitochondria. The resulting mitochondria-bound proteins were processed and analyzed as in panel B. D, the *in vitro* synthesized radioactive single-cysteine Bcl-XL and Bax proteins were incubated in the absence or presence of the MOM liposomes and/or the BH3 peptide. The resulting proteoliposomes were processed and analyzed as in panel A. In all panels, the labels are as described in Figure 1. In addition, filled or open triangles indicate the disulfide-linked Bcl-XL or Bax homodimers, and stars or squares indicate the disulfide-linked Bcl-XL or Bax:mitochondrial protein complexes, respectively. The NEM-Mito in panel B indicates that the mitochondria used in the reaction were pretreated with NEM to block the sulfhydryl moieties in the mitochondrial proteins preventing their crosslinking with the sulfhydryl moieties in the Bcl-XL and Bax proteins.

**Figure 8. A model for the parallel helix 1:helix 1 dimer interface in the membrane-bound Bcl-XL:Bax heterodimer.** A, *Left panel*, to build the initial model, the helix 1 extracted from the Bax monomer structure (PDB ID: 1F16) was manually positioned onto the helix 1 of the Bcl-XL protein in the Bcl-XL protein:Bax BH3 peptide complex structure (PDB ID: 3PL7) such that the three cysteine pairs, E7C–M20C, S18C–F30C, and S23C–R34C which resulted in disulfide-linked Bcl-XL:Bax heterodimers in Figure 7, are in a geometry suitable for disulfide linkage. The resulting complex structure was inputted into FlexPepDock program and one of the top ten output models is shown with the cysteine pairs presented in stick form and their gamma sulfur atoms (S<sub>1</sub><sup>γ</sup> and S<sub>2</sub><sup>γ</sup>) linked by virtual bonds and the distances in Å indicated. The C<sub>1</sub><sup>β</sup>–S<sub>1</sub><sup>γ</sup>–S<sub>2</sub><sup>γ</sup>–C<sub>2</sub><sup>β</sup> dihedral angles about the disulfide bond for the three cysteine pairs are +99.2°, +114.5° and -178.6°, respectively. *Right panel*, to generate the final model, the cysteines in the left panel were changed back to the corresponding wild-type residues. The resulting complex structure was the starting model in an automated peptide docking experiment with FlexPepDock program. One of the top ten output models from the docking experiment is shown with the respective wild-type residue pairs presented in stick form and their beta carbon atoms (C<sub>1</sub><sup>β</sup> and C<sub>2</sub><sup>β</sup>) linked by dashed lines with the distances in Å indicated. B, a model for the parallel helix 1:helix 1 interface in the Bcl-XL:Bax heterodimer was built based on the model presented in the right panel of (A) and the photocrosslinking data shown in Figure 6. The residues that generated the heterodimer-specific photoadducts when replaced by ANB-lysine are presented in stick form. In all models, the BH1-4 regions of Bcl-XL protein are colored as in Figure 5, and the helix 1 of Bax is colored magenta. For simplicity, the BH3 helix of Bax was omitted from the models.

**Figure 9. Disulfide crosslinking of Bax and Bcl-XL proteins with a single cysteine in their helix 1 that supports the antiparallel helix 1:helix 1 dimer model.** A, the *in vitro* synthesized [<sup>35</sup>S]Met-labeled single-cysteine Bcl-XL and Bax proteins were activated by the BH3 peptide and targeted to the MOM liposomes. The resulting membrane-bound proteins were processed and analyzed as described in Figure 7. B, the antiparallel helix 1:helix 1 dimer model was based on the disulfide crosslinking data from two single-cysteine Bcl-XL–Bax mutant pairs, E7C–R34C and S23C–M20C, shown in panel A. It was generated by FlexPepDock program and presented similarly as described in Figure 8A. *Left panel*, the

two cysteine pairs are presented in stick form with their gamma sulfur atoms ( $S_1^\gamma$  and  $S_2^\gamma$ ) linked by virtual bonds and the distances in Å indicated. The  $C_1^\beta$ - $S_1^\gamma$ - $S_2^\gamma$ - $C_2^\beta$  dihedral angles about the disulfide bond for the two cysteine pairs are  $+146.7^\circ$  and  $-74.0^\circ$ , respectively. *Right panel*, the two respective wild-type residue pairs are presented in stick form with their beta carbon atoms ( $C_1^\beta$  and  $C_2^\beta$ ) linked by dashed lines and the distances in Å indicated. The BH1-4 regions of Bcl-XL protein and the helix 1 of Bax are colored as in Figure 8. For simplicity, the BH3 helix of Bax was omitted from the models.

**Figure 10. Effects of interfacial mutations on Bcl-XL:Bax heterodimer formation and function.** *A*, a part of the crystal structure of Bcl-XL protein:Bax BH3 peptide complex (PDB ID: 3PL7) is shown in the left panel with Bcl-XL Gly<sup>138</sup> changed to alanine (G138A) and Arg<sup>139</sup> changed to aspartate (R139D), and in the right panel with Bax Met<sup>74</sup> changed to glutamate (M74E). The mutated residues are shown in stick form. The residues in the respective binding partners that interact with these mutated residues are also illustrated in stick form with dashed lines linking the  $C^\beta$  of Bcl-XL Ala<sup>138</sup> to the backbone carbonyl O of Bax Gly<sup>67</sup>,  $O^{\delta 1}$  of Bcl-XL Asp<sup>139</sup> to  $O^{\delta 1}$  of Bax Asp<sup>68</sup>, and the  $C^\gamma$  of Bax Glu<sup>74</sup> to  $C^{\epsilon 2}$  of Bcl-XL Tyr<sup>195</sup>. The distances between these atoms are indicated in Å. *B-D*, the *in vitro* synthesized [<sup>35</sup>S]Met-labeled single-cysteine Bcl-XL and Bax proteins with or without the indicated interfacial mutations were activated by the BH3 peptide and targeted to the Bax<sup>-</sup>/Bak<sup>-</sup> mitochondria that were either untreated (*B*) or pretreated with NEM (*C-D*). The mitochondria-bound proteins were processed and analyzed as described in Figure 3. *E*, the indicated Bax proteins were synthesized *in vitro*, and their BH3 peptide-dependent cytochrome c release activities in the Bax<sup>-</sup>/Bak<sup>-</sup> mitochondria were assayed in the absence or presence of the indicated *in vitro* synthesized Bcl-XL proteins as described in Figure 2. Data shown are average fractions of cytochrome c release from two to four independent experiments with the ranges indicated by error bars.

**Figure 11. Effects of ABT-737 on interactions and MOMP activity of Bcl-XL and Bax.** *A-C*, the indicated *in vitro* synthesized [<sup>35</sup>S]Met-labeled single-cysteine Bax (*A*), Bax and Bcl-XL (*B-C*), or Bax and Bcl-XL R139D (*B*) proteins were activated by the BH3 peptide and targeted to the MOM liposomes in the absence or presence of ABT-737, purified non-radioactive recombinant Bcl-XL protein (rBcl-XL), or both. The resulting proteoliposomes were processed and analyzed as described in Figures 3. *D*, cytochrome c release from the Bax<sup>-</sup>/Bak<sup>-</sup> mitochondria by the indicated single-cysteine Bax proteins synthesized *in vitro* was assayed in the absence or presence of the BH3 peptide, the indicated single-cysteine Bcl-XL protein synthesized *in vitro*, and/or ABT-737 as described in Figure 2. Data shown are average fractions of cytochrome c release from two to six independent experiments with the ranges indicated by error bars.

**Figure 12. IASD-labeling of single-cysteine Bax and Bcl-XL proteins in liposomal membranes.** The [<sup>35</sup>S]Met-labeled mutants with a single cysteine positioned in the following regions, helix 1 and BH1-3 groove of Bcl-XL (*A*), helix 1 and BH3 helix of Bax (*B*), helices 5, 6, and 9 of Bax (*C, top panel*) or of Bcl-XL (*D, top panel*), were synthesized in the wheat germ-based *in vitro* system. The resulting radioactive Bcl-XL or Bax protein, either alone or together with the purified non-radioactive recombinant Bax (rBax) or Bcl-XL (rBcl-XL) protein, respectively, were activated by the BH3 peptide and targeted to the MOM liposomes. The resulting proteoliposomes were isolated and treated with IASD in the absence or presence of CHAPS, urea, or both. After 30 min, the labeling reactions were stopped by β-mercaptoethanol. For the “0 min” controls, the samples were pretreated with β-mercaptoethanol before addition of IASD. The resulting radioactive proteins were resolved using IEF and detected by phosphor-imaging. Circles and triangles indicate the unlabeled and IASD-labeled Bcl-XL proteins, and square and angle brackets indicate the unlabeled and IASD-labeled Bax, respectively. The phosphor-imaging data for IASD labeling of radioactive Bcl-XL and Bax mutants in the top panels of (*C-D*) and the similar data

from one to four independent replicates were quantified. In the corresponding bottom panels, the average fractions of IASD labeling for the mutants under the specified conditions are presented as bar graphs of the specified patterns with the ranges indicated by error bars. *E*, the indicated [<sup>35</sup>S]Met-labeled Bax mutants were synthesized in the wheat germ (WG)- or rabbit reticulocyte lysate (RRL)-based *in vitro* translation system, and analyzed with IEF and phosphor-imaging. The K119C or D142C mutant was constructed from the C0 mutant by changing Lys<sup>119</sup> or Asp<sup>142</sup> to cysteine, respectively.

Figure 13. **Photocrosslinking of Bcl-XL and Bax proteins with a single photoreactive ANB-lysine incorporated in the membrane-embedded helices.** The *in vitro* synthesized [<sup>35</sup>S]Met-labeled Bcl-XL (*A*) or Bax (*B*) protein with the photoreactive probe attached to the indicated single lysine in the helix 5, 6 or 9 was activated together with purified 6H-Bax (*A*) or 6H-Bcl-XL (*B*) protein, respectively, by the BH3 peptide and targeted to the MOM liposomes. The resulting proteoliposomes were processed and analyzed as described in Figure 4.

Figure 14. **Chemical crosslinking of single-cysteine Bcl-XL and Bax proteins.** The indicated *in vitro* synthesized [<sup>35</sup>S]Met-labeled single-cysteine Bcl-XL and Bax proteins were activated by the BH3 peptide and targeted to the MOM liposomes. The resulting proteoliposomes were isolated and subjected to BMH crosslinking. The resulting radioactive proteins and their adducts were analyzed by reducing SDS-PAGE and phosphor-imaging. Arrows indicate the BMH-crosslinked heterodimers. Other labels are the same as those in Figure 3.

Figure 15. **A model for the overall structural organization of the Bcl-XL:Bax heterodimer in membranes.** The cytosolic part of the heterodimer model was assembled by merging the BH1-3 groove: BH3 helix interface model (Fig. 5A) with the parallel helix 1: helix 1 interface model (Fig. 8A, right panel). The MOM-embedded part was assembled with the alpha helix 9 ( $\alpha$ 9) of Bcl-XL and the alpha helices 5, 6 and 9 ( $\alpha$ 5,  $\alpha$ 6 and  $\alpha$ 9) of Bax. The distances between these membrane-embedded helices were set according to the BMH crosslinking data (Fig. 14). The distances between the helix  $\alpha$ 8 or  $\alpha$ 9 of Bcl-XL and the BH3 helix ( $\alpha$ BH3) or helix  $\alpha$ 4 of Bax, respectively, were further adjusted based on the BMH crosslinking data. Dashed lines link the residues that were crosslinked by BMH when they were mutated to cysteines. The residues shown as spheres are embedded in the MOM, because their cysteine substitutions could not be substantially labeled by IASD unless CHAPS was added (Fig. 12). The residues shown as sticks are exposed to the cytosol, because their cysteine substitutions could be labeled by IASD in the absence of CHAPS and urea.

## Figure 1

### A. Bax Single Cysteine Mutants

```

MDGSGEQPRGGGPTSSEQIMKTGALLQ 28
                                helix 1
GFIQDRAGRMGGEAPELALDPVPQDAST 56
    ----- BH3 -----
KKLSECLKRIGDELDSNMELQRMIAAVDT 85
    helix 2          ▲ helix 3          BH1
DSPREVFFRVAADMFSDGNFNWGRVVAL 113
    ----- helix 4 -----
FYFASKLVLKALCTKVPELIRTIMGWTLDF 143
    helix 5          BH2          helix 6
LRERLLGWIQDQGGWDGLLSYFGTPTWQ 171
    helix 7          helix 8
TVTIFVAGVLTASLTIWKKMG 192
    ----- helix 9 -----
    
```

### B. Bcl-XL Single Cysteine Mutants

```

MSQSNRELVDFLSYKLSQKGYSWSQFS 28
                                BH4
                                helix 1
DVEENRTEAPEGTESEMETPSAINGNPS 56

WHLADSPAVNGATGHSSSLDAREVIPMAA 85
    ----- BH3 -----
VKQALREAGDEFELRYRRAFSDLTSQLHIT 115
    helix 2          BH1          helix 3
PGTAYQSFEQVVNELFRDGVNWGRIVAFF 144
    ----- helix 4 -----
SFGGALCVESVDKEMQVLVSRIAAWMATY 173
    helix 5          BH2          helix 6
LNDHLEPWIQENGGWDTFVELYGNNAAA 201
    helix 7          helix 8
ESRKGQERFNRWFLTGMTVAGVVLLGSLF 230
    ----- helix 9 -----
SRK 233
    
```

### C. Bcl-XL Single Lysine Mutants

```

MSQSNRELVDFLSYKLSQKGYSWSQFS 28
                                BH4
                                helix 1
DVEENRTEAPEGTESEMETPSAINGNPS 56

WHLADSPAVNGATGHSSSLDAREVIPMAA 85
    ----- BH3 -----
VKQALREAGDEFELRYRRAFSDLTSQLHIT 115
    helix 2          BH1          helix 3
PGTAYQSFEQVVNELFRDGVNWGRIVAFF 144
    ----- helix 4 -----
SFGGALCVESVDKEMQVLVSRIAAWMATY 173
    helix 5          BH2          helix 6
LNDHLEPWIQENGGWDTFVELYGNNAAA 201
    helix 7          helix 8
ESRKGQERFNRWFLTGMTVAGVVLLGSLF 230
    ----- helix 9 -----
SRK 233
    
```

Figure 2

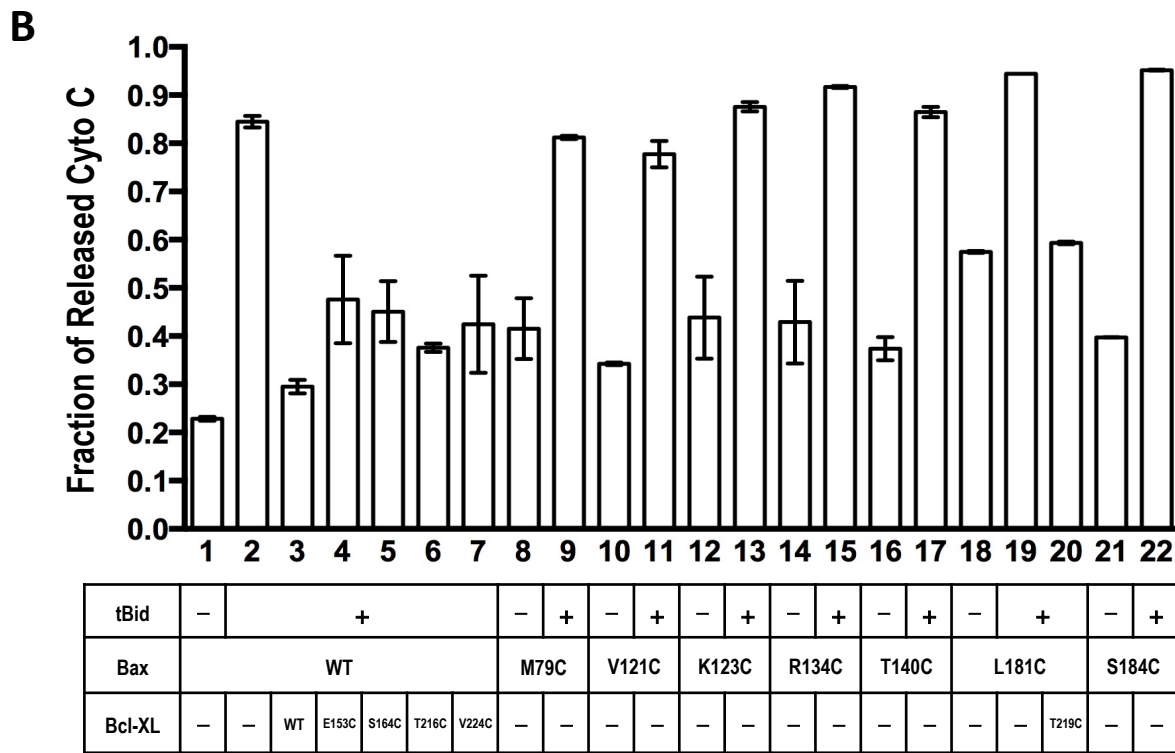
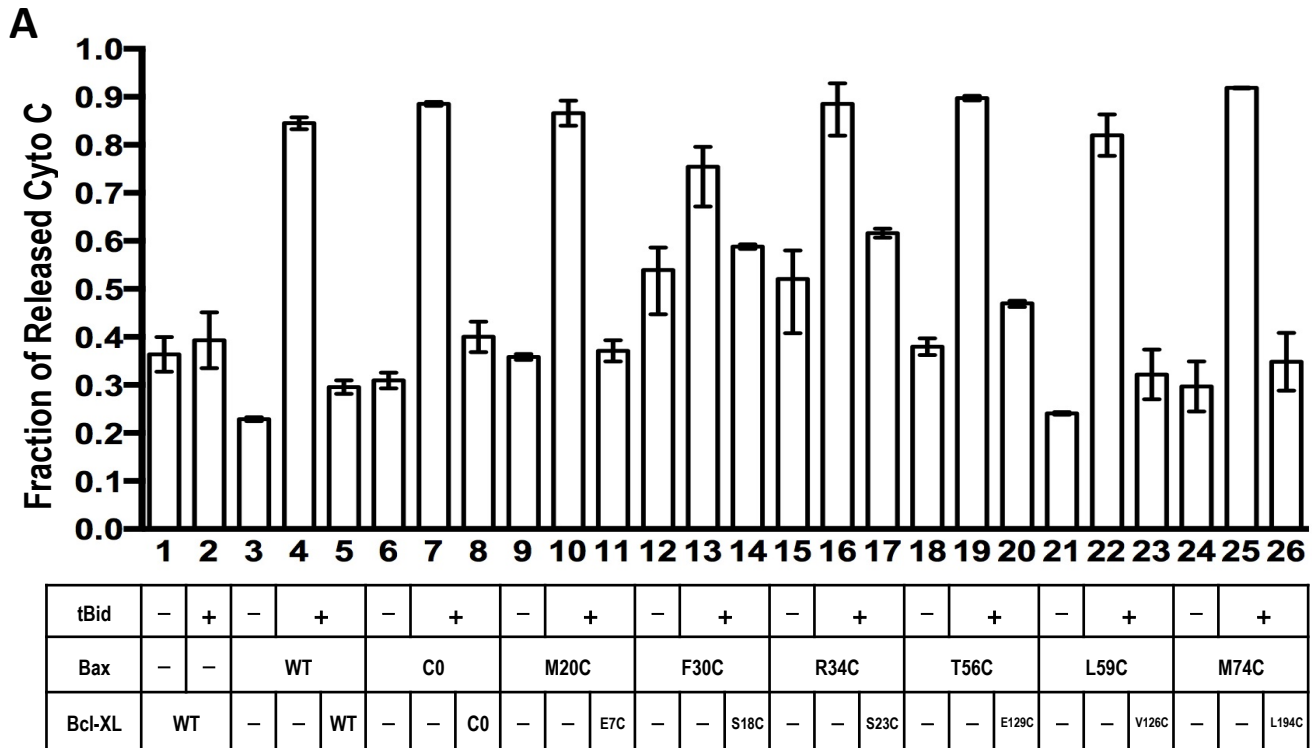
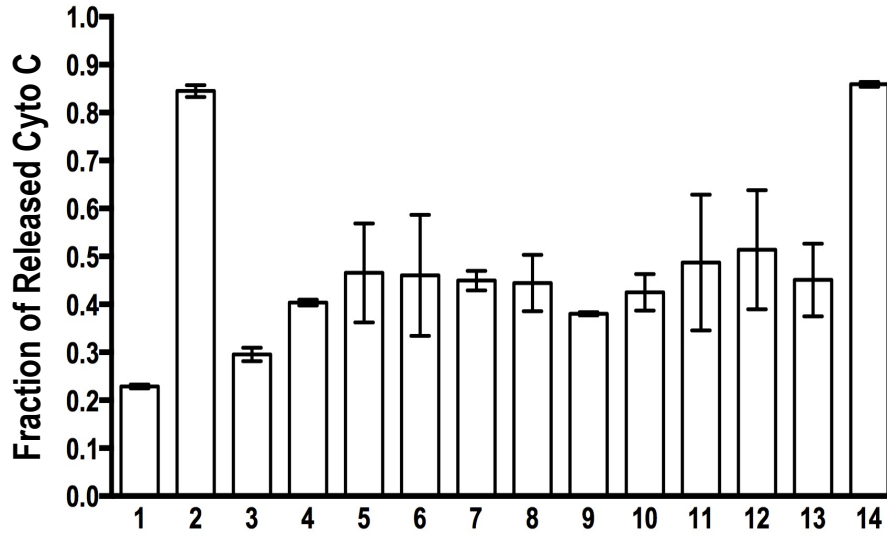


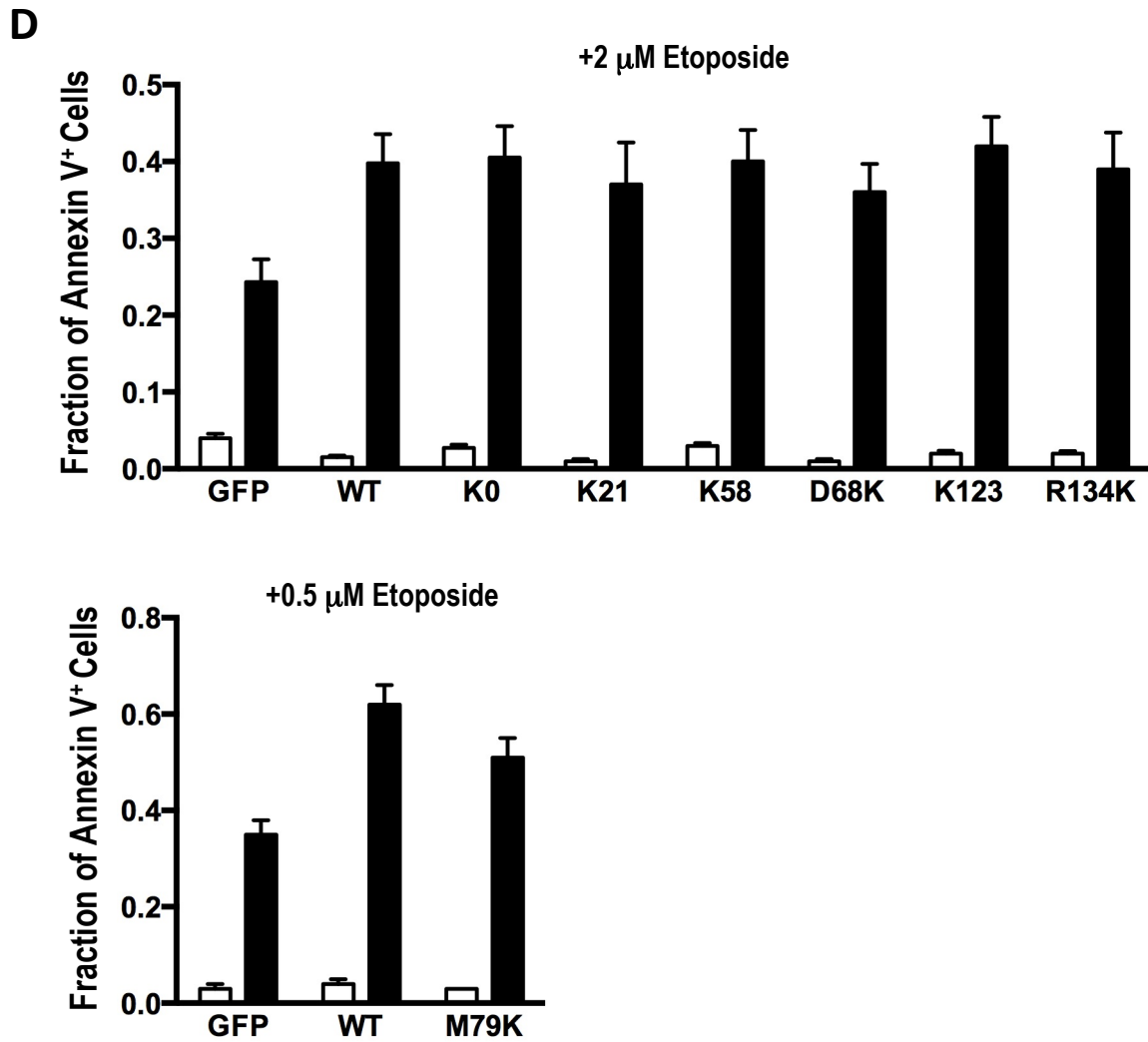
Figure 2 (Continue)

C



tBid	-	+											-	+
Bax	WT												A183K	
Bcl-XL	-	-	WT	K0	R6K	K16	F97K	Q111K	Q125K	E129K	R212K	T219K	-	-

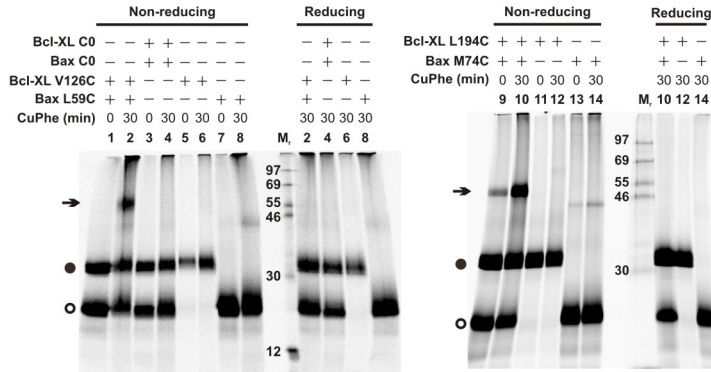
Figure 2 (Continue)



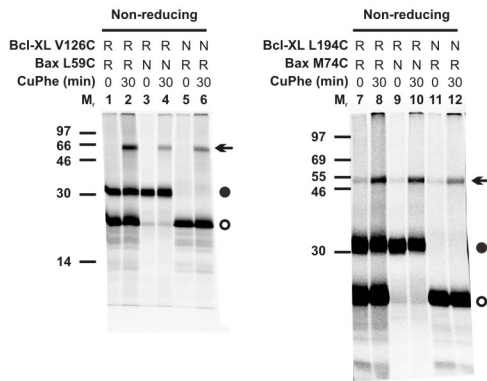
Architecture of antiapoptotic Bcl-XL:Bax dimer in membranes

Figure 3

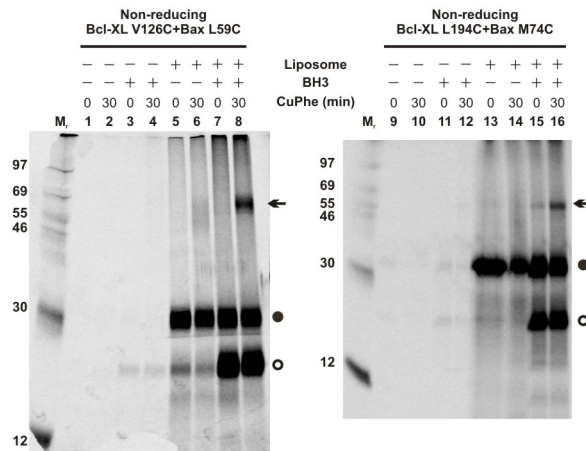
A



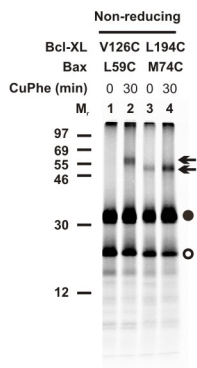
B



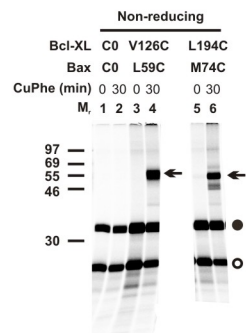
C



D



E



F

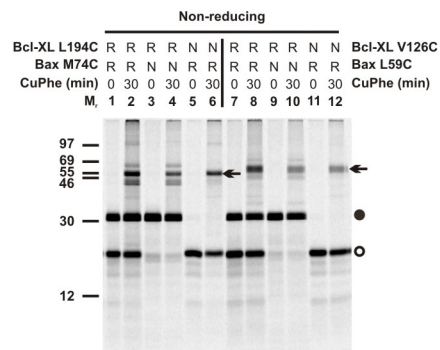
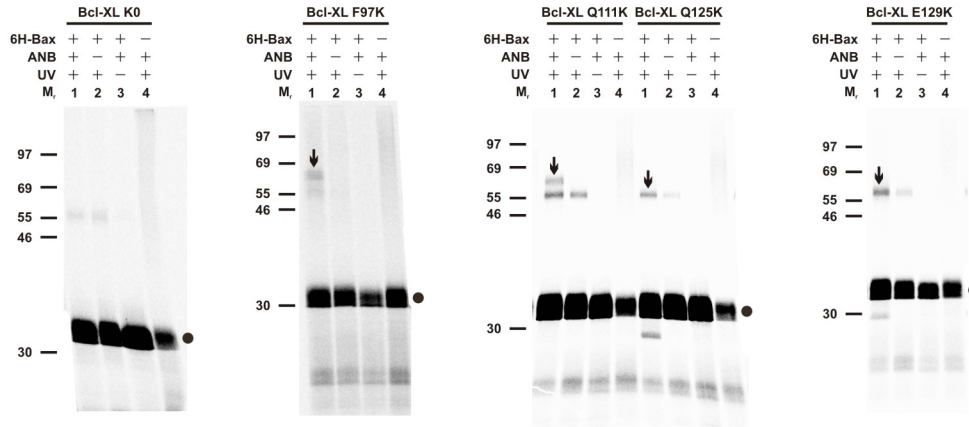


Figure 4

A



B

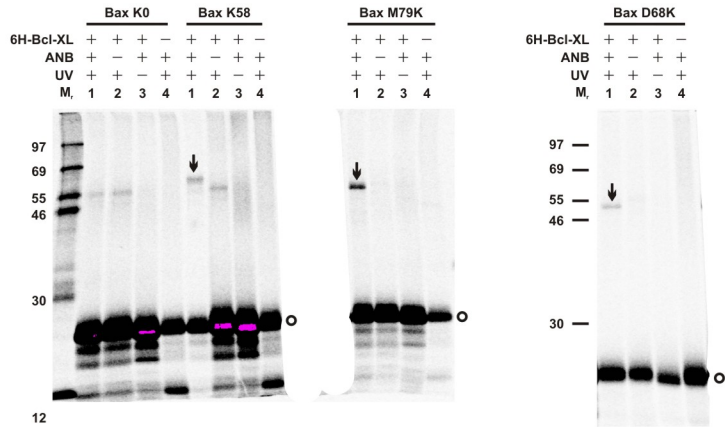


Figure 5

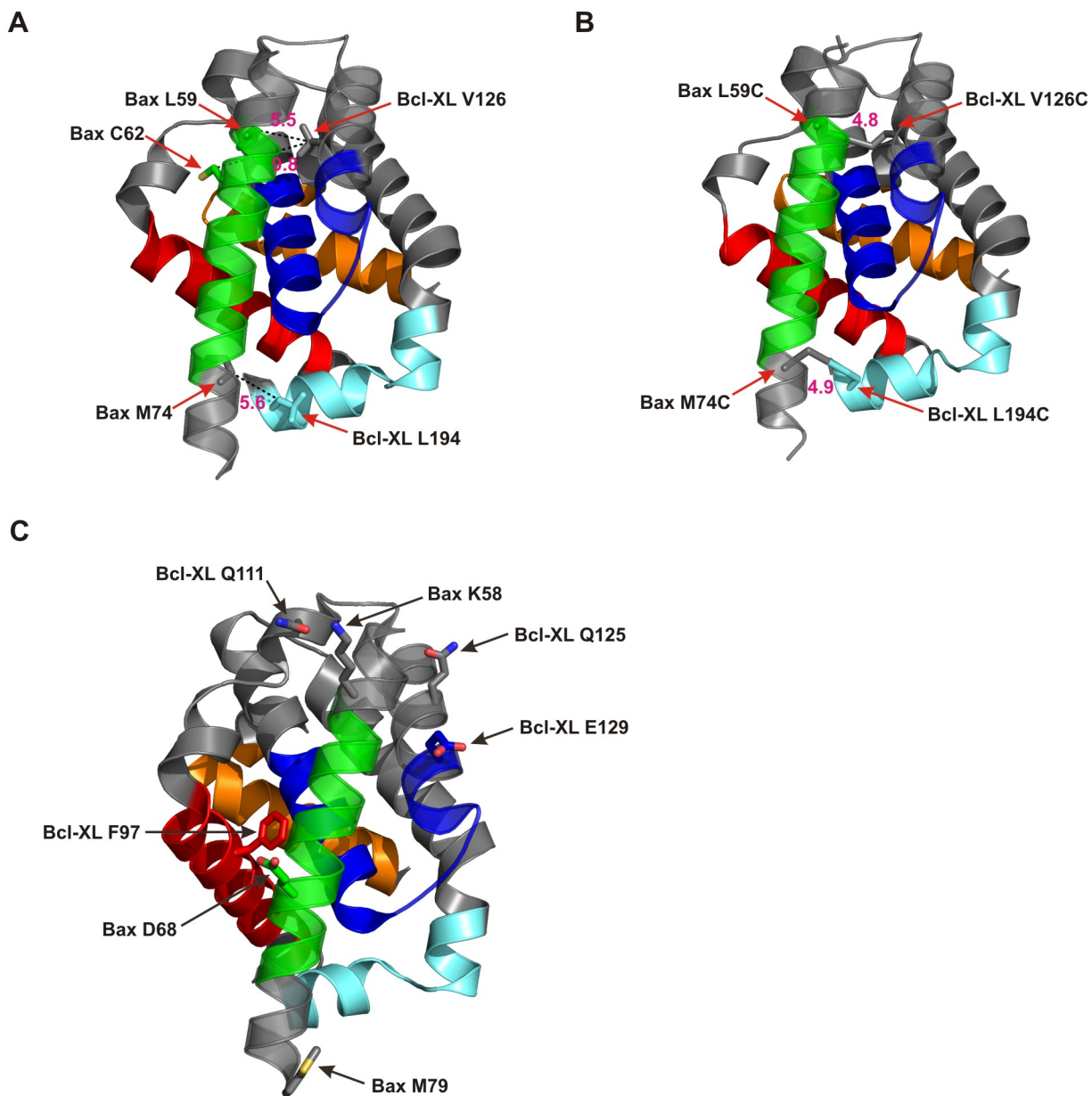


Figure 6

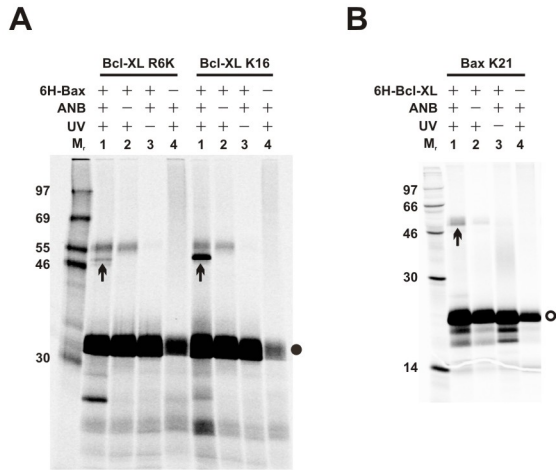


Figure 7

Architecture of antiapoptotic Bcl-XL:Bax dimer in membranes

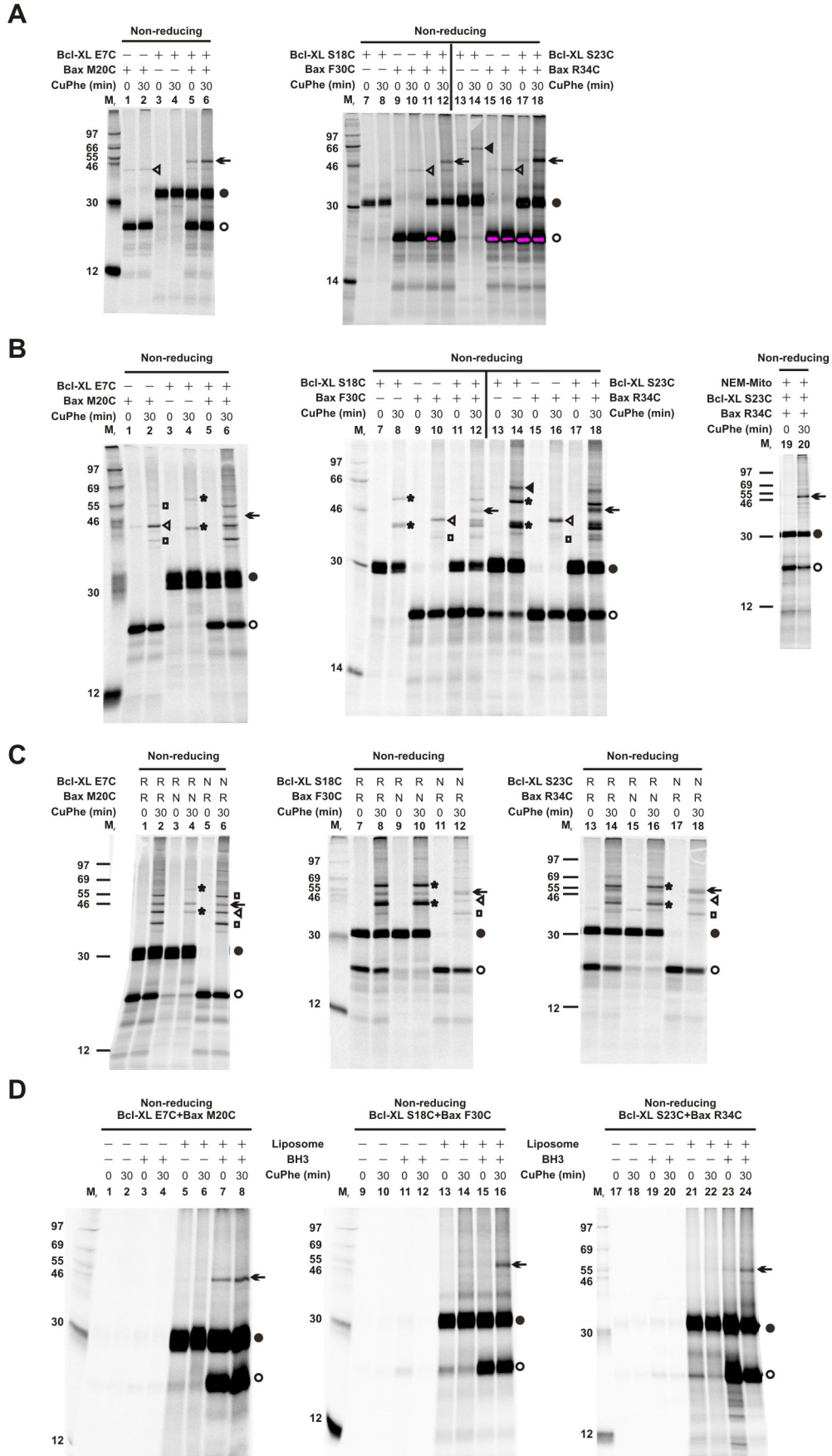
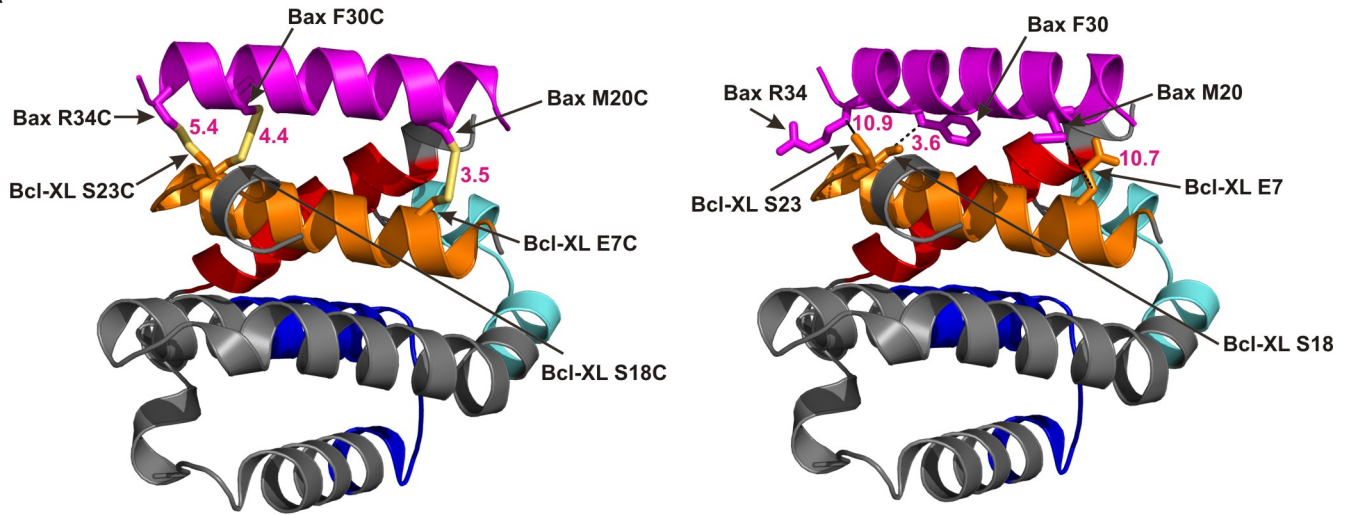


Figure 8

A



B

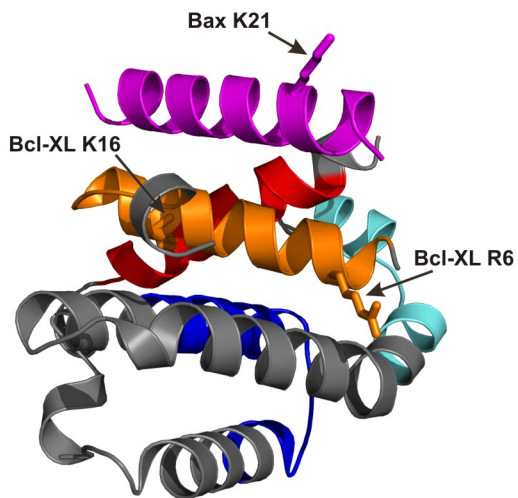
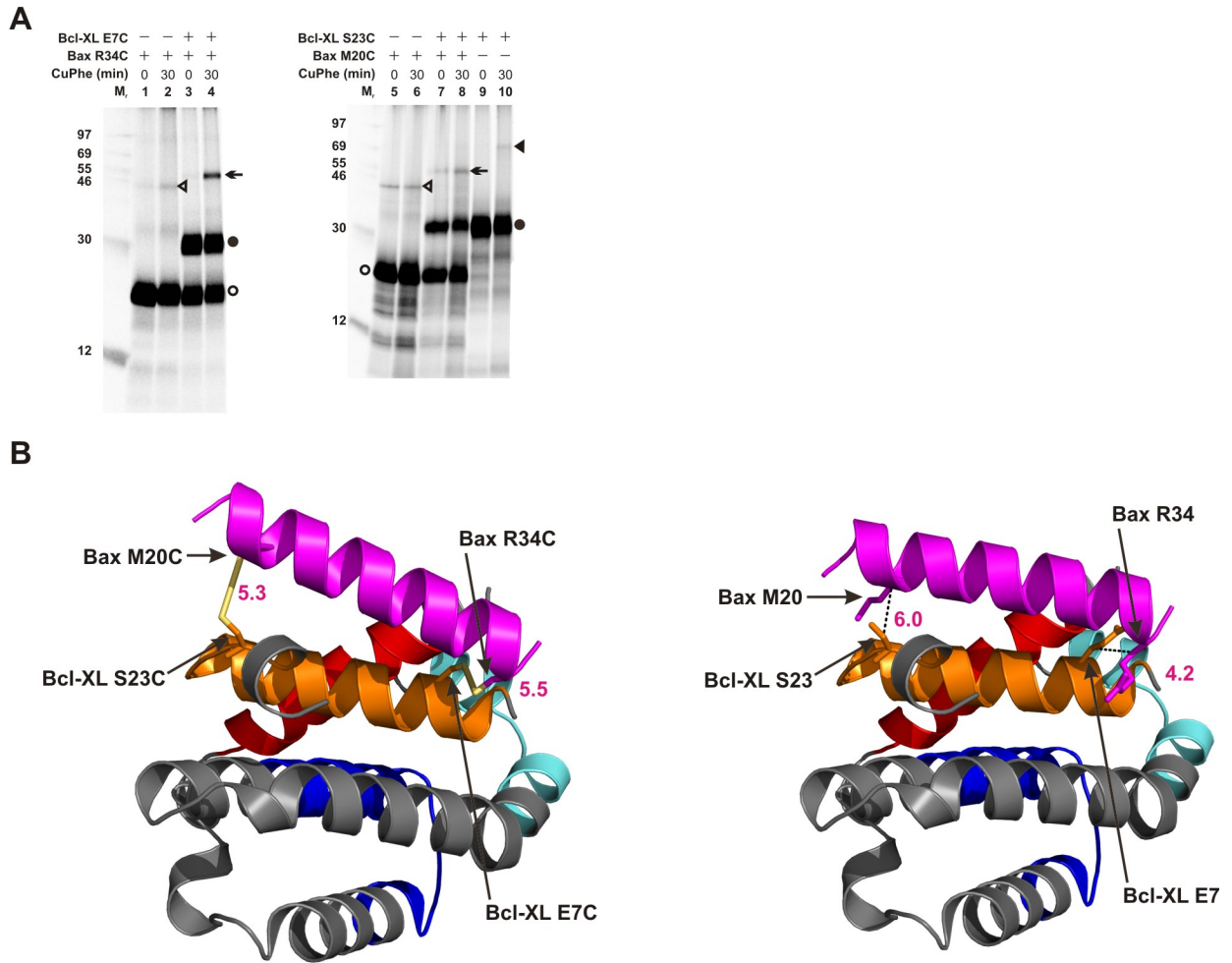


Figure 9



Architecture of antiapoptotic Bcl-XL:Bax dimer in membranes

Figure 10

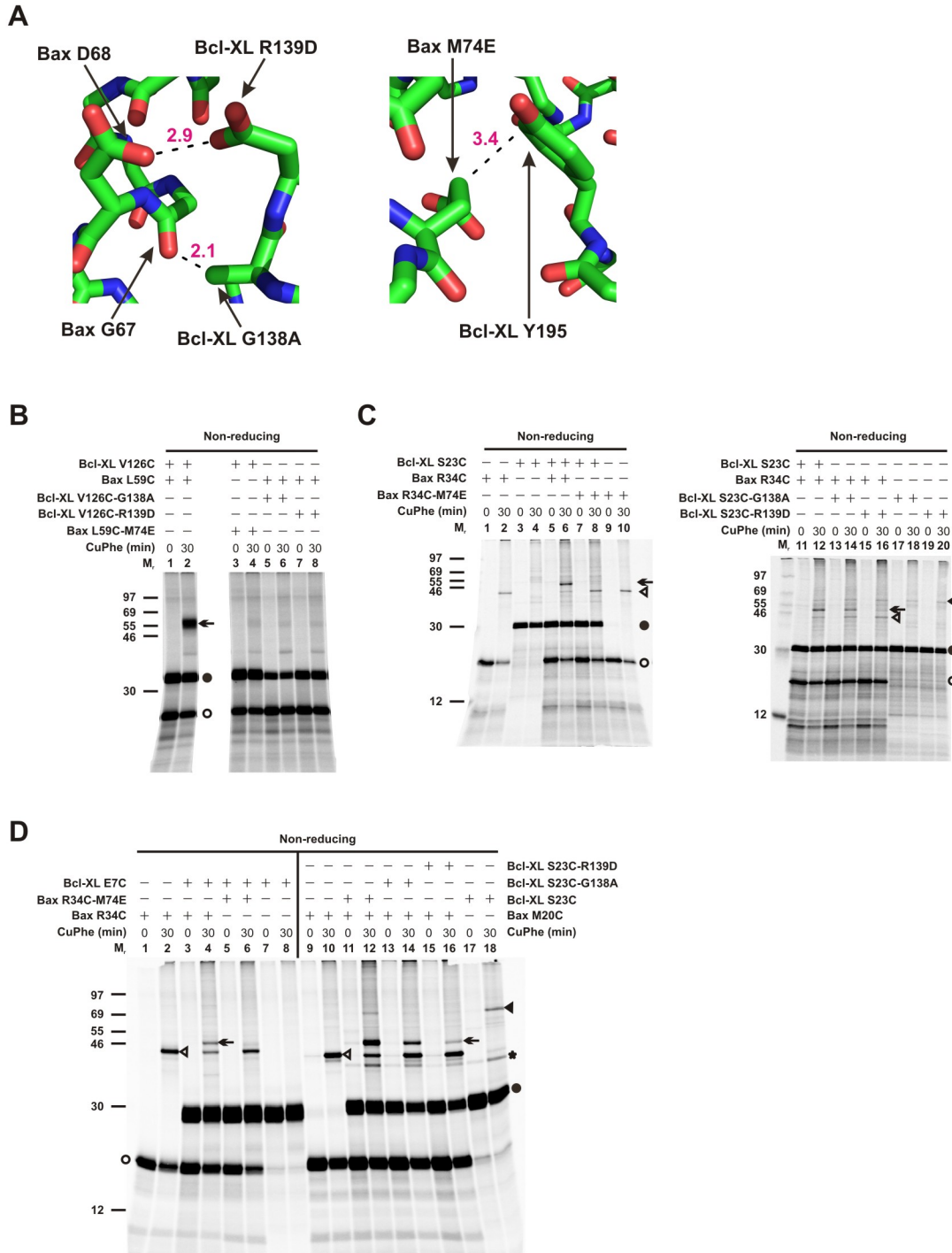


Figure 10 (Continue)

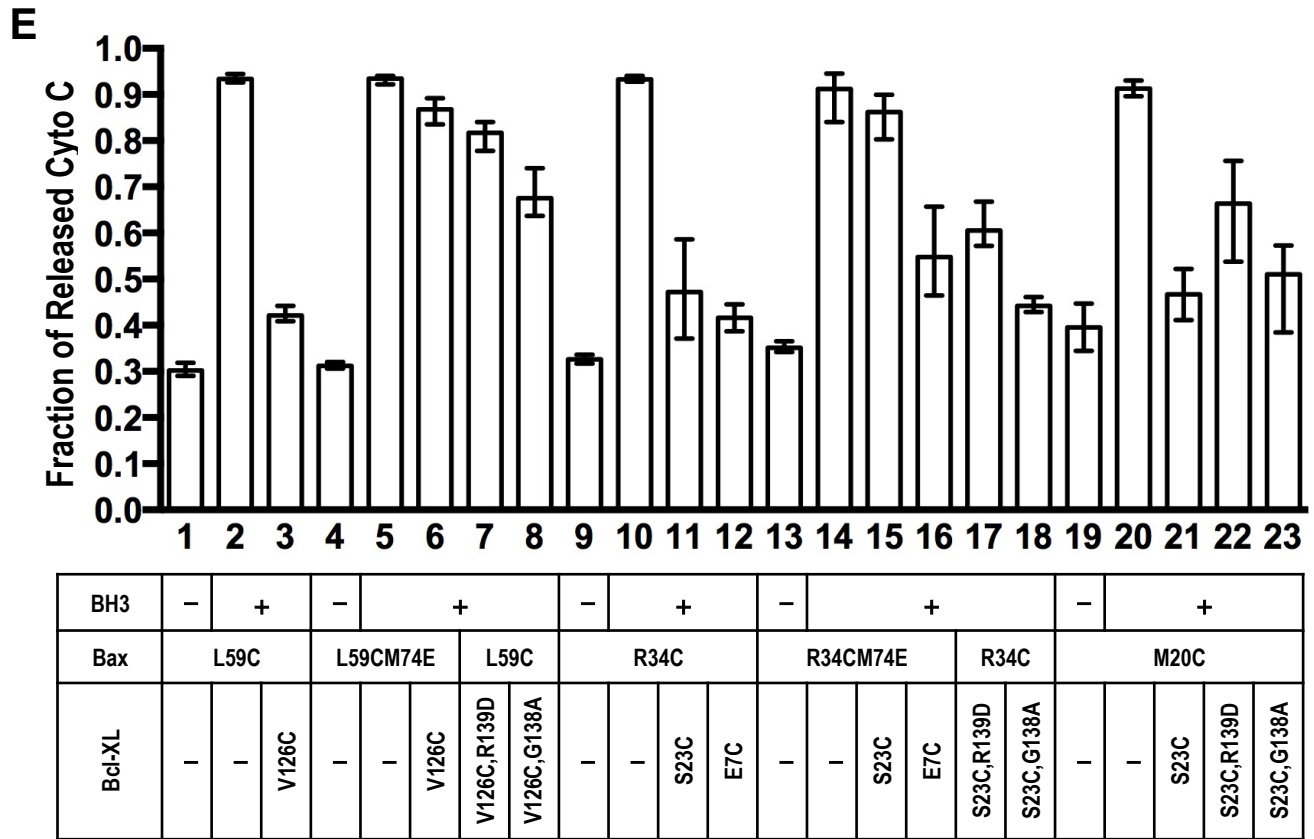
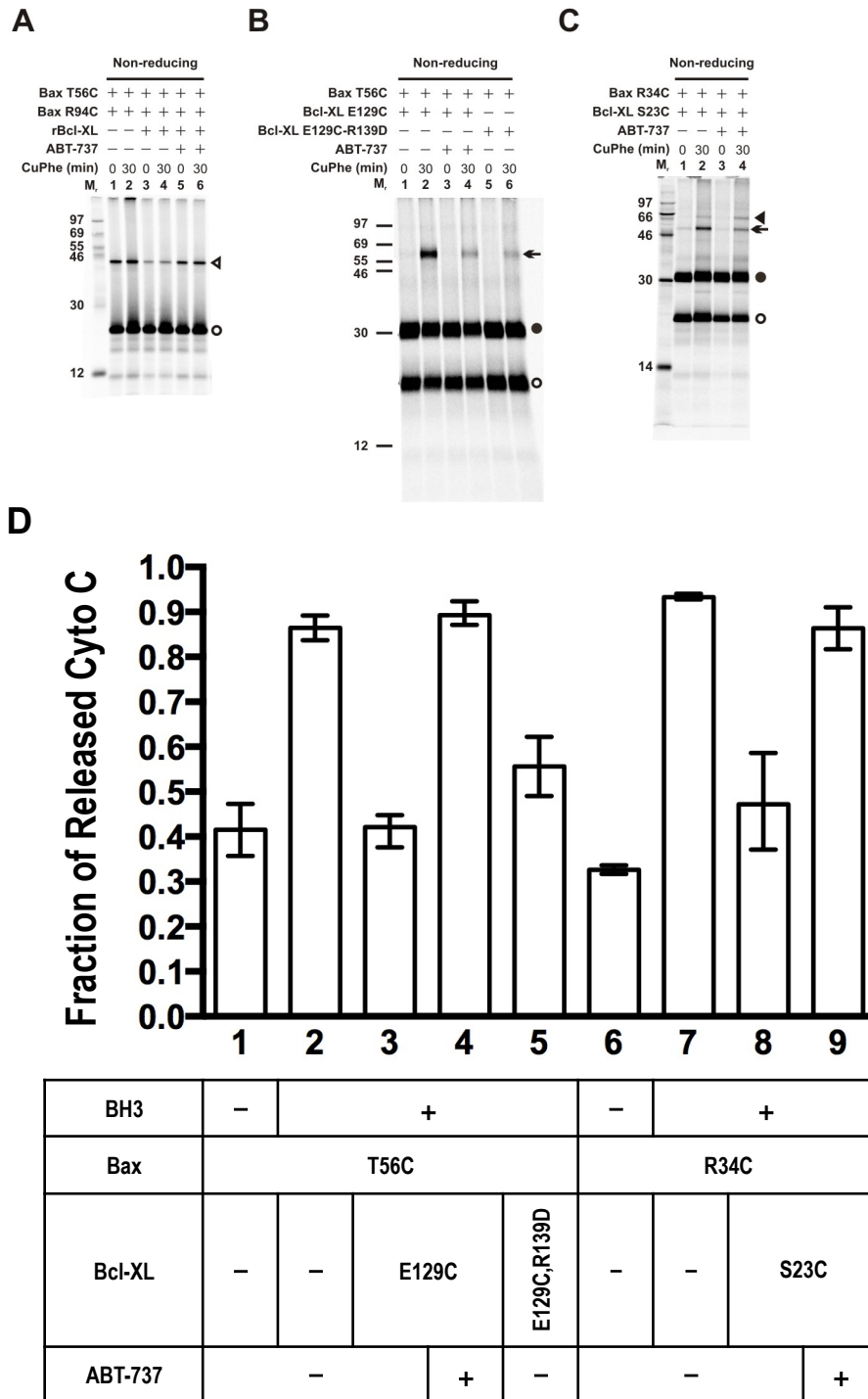
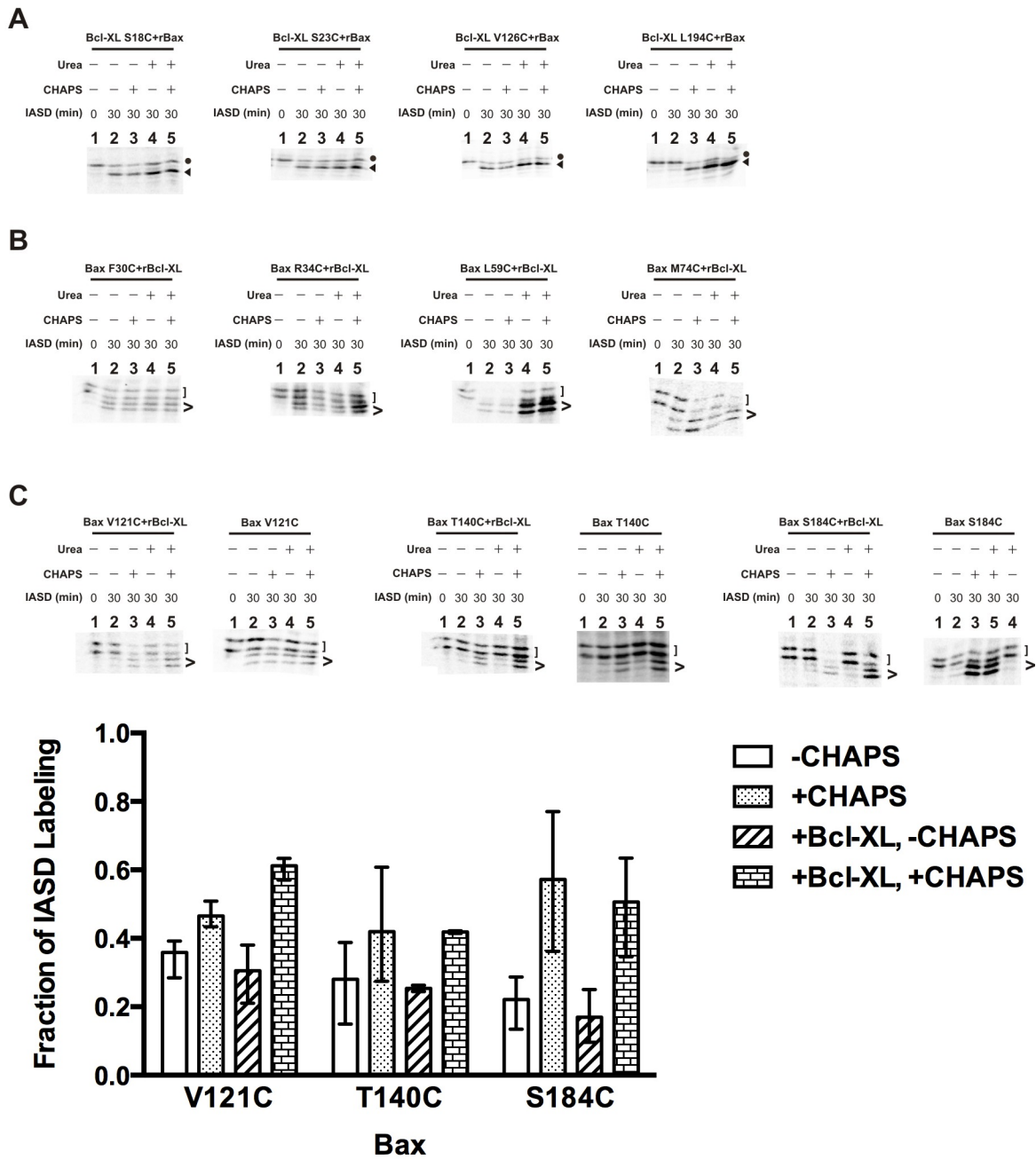


Figure 11



Architecture of antiapoptotic Bcl-XL:Bax dimer in membranes

Figure 12



Architecture of antiapoptotic Bcl-XL:Bax dimer in membranes

Figure 12 (Continue)

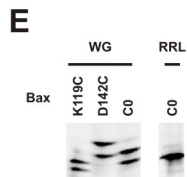
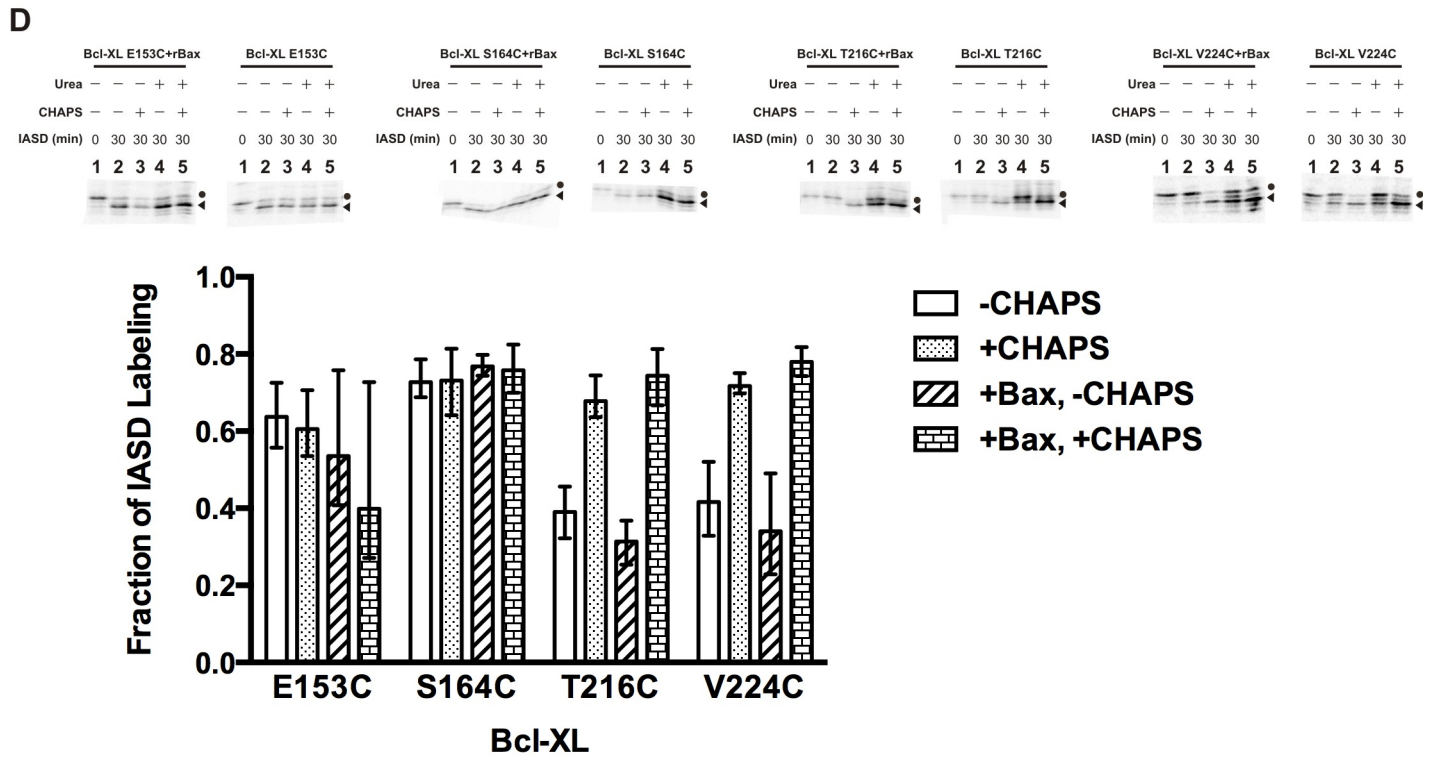


Figure 13

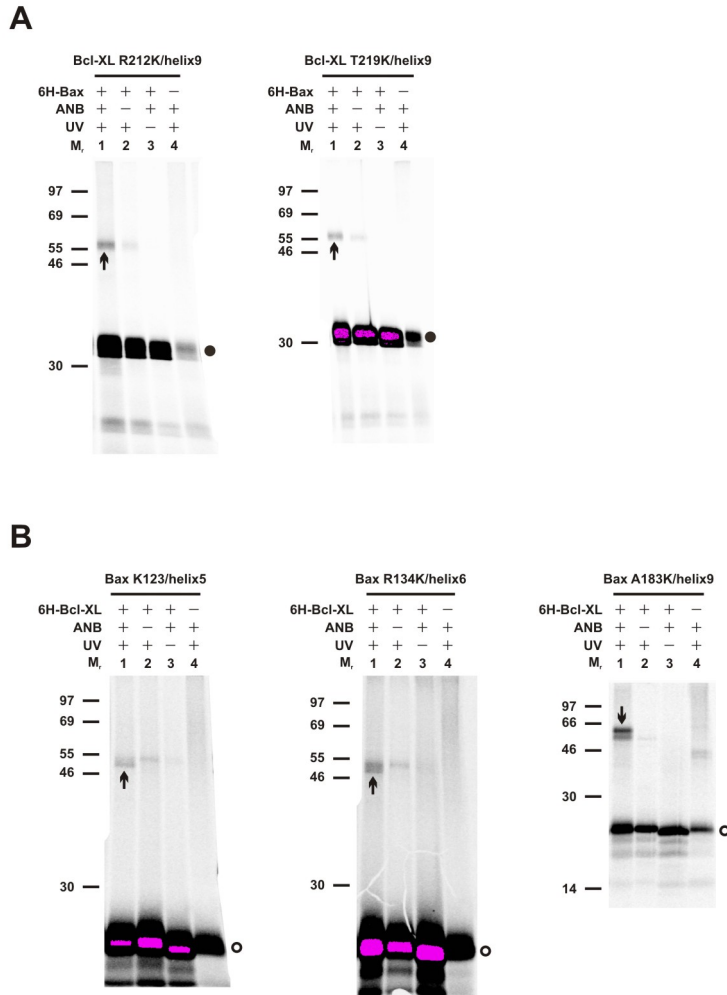
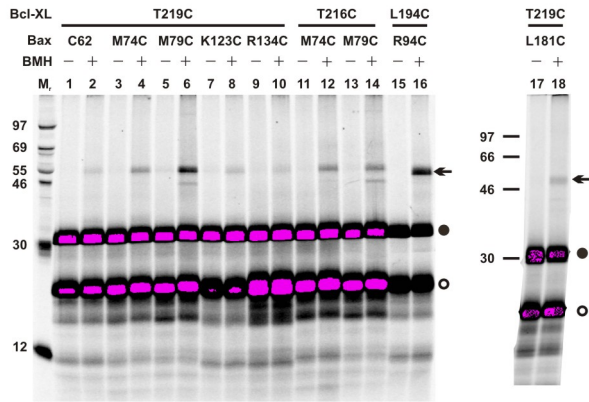


Figure 14



Architecture of antiapoptotic Bcl-XL:Bax dimer in membranes

Figure 15

